Universidad Tecnológica de Pereira

MASTER OF SCIENCE IN ELECTRICAL ENGINEERING

THESIS

Integration of photovoltaic solar generation systems with energy storage for improving electric power quality

Mario Alejandro Useche Arteaga

Supervisor
Professor, Alejandro Garces Ruíz

2020

Summary

This thesis presents control strategies for photovoltaic and energy storage systems with the aim to improve voltage profiles, compensate harmonics and improve frequency response. Model predictive control (MPC) and finite control set model predictive control (FCS-MPC) are considered. These controls are integrated into the conventional cascade structure of vector oriented control which is the most common approach in commercial systems. In this way, the proposed control is easily implemented in practice following standard procedures in the industry.

On the other hand, the concept of virtual synchronous machine is reviewed and applied through the control of the active power of the energy storage system and taking advantage of the $P - V^2$ relationship of the capacitor of the dc-link of the voltage source converter.

The control strategies are simulated in MATLAB/SIMULINK using realistic test distribution systems based on the Colombian context. The proposed controls show clear advantages over conventional control of photovoltaic systems and improve the power quality of the system.

Acknowledgments

I would like to express my sincere gratitude to my advisor Alejandro Garces for his rewarding support of my master's degree and research process, for his patience, motivation, enthusiasm, and knowledge. His guidance helped me in all the time of research and writing of this thesis.
I also gratefully acknowledge the technical and financial support received towards this process from Empresa de Energía del Quindío and Universidad tecnológica de Pereira, my coworkers, classmates and all friends for had taken time to discuss, gave me ideas to enrich my work and encouragement during my years of study and research.
Finally, I must express my very profound gratitude to my family for unconditional support and continuous encouragement through the process of my master's degree. This accomplishment would not have been possible without them.

Contents

Chapter 1

Introduction

1.1 Motivation

Photovoltaic (PV) solar generation is an environmentally-friendly alternative to conventional sources such as oil, coal, and natural gas; however, the control of PV systems is usually oriented to the active power leaving aside the reactive power and wasting the capability of the converter for improving the power quality of the grid. On the other hand, the high level of integration of solar generation has caused a decrease in the inertia of modern power systems. This fact represents great challenges in terms of stability, power quality, and reliability. Connection points with low short-circuit capacity also known as electrically weak networks, severely affect the ability to supply energy. These problems are related to the control of the converters and not to the power electronics.

Solar PV systems are integrated into the grid through a voltage source converter. This type of converter can inject or consume reactive power, however, it is usually operated at a unity power factor. This creates problems of voltage deviations that must be corrected voltage regulator with tap changers under load (OLTC) usually placed in the substations. Static var compensator (SVC) and static synchronous compensator (STATCOM) can be also implemented in modern power distribution systems to compensate for these deviations. However, a suitable control strategy in the solar PV system can reduce the requirement of these components.

On the other hand, PV systems usually include banks of batteries that are also controlled by power converters and can be used to improve power quality. This includes harmonics compensation and frequency control. However, it is necessary to modify the control of the PV system without affecting the other objectives of control inherent in the system; for that reason, this thesis proposes a model predictive control and a finite control set model predictive control (FCS-MPC) which allows multi-objective controls.

Additionally, power quality is a complex problem in modern power distribution systems due to intrinsic characteristics, such as unbalance, different conductors along the system, radial topology with multiple branches, load centers located at long electric distances, and high penetration of PV systems. On the other hand, power electronics converters, commonly used in industrial processes, introduce harmonic currents, affecting power quality and reducing the efficiency of the entire grid. Industrial loads are currently sensitive to power quality problems such as voltage events and harmonics, and that is the reason why an energy supply with high-quality standards is necessary. However, the continuous growth of renewable systems has created grids with low short-circuit capacity. Therefore, the grid may produce drops of voltage and frequency at the moment of electric faults or the starting of induction motors.

1.2 State of the art

1.2.1 Control of power electronic converters for photovoltaic systems

Conventional photovoltaic (PV) systems use voltage source converters and vector oriented control (VOC) for integrating the power generated by the PV modules into the ac grid. Voltage source converter (VSC) is a six pulse converter consisting of six power semiconductor switching devices (GTO, IGCT, IGBT, etc) with a dc capacitor at the dc side and a filter in the ac side (Chapter 2 will present more details). The classic control of VSCs combines PI regulators, Park/Clark transformation, pulse width modulation (PWM), and grid synchronization for controlling the VSC and apply vector control. The dc side has a capacitor that is responsible for regulating the dc voltage and weakens the impacting current during switching controlled by the outer loop usually with a PI control which controls reactive power (Song et al., 2005).

In order to improve the performance of the systems, different control techniques have been proposed such as modified versions of space vector modulation (SVM), sliding mode control(SMC), and multilevel voltage source converters. SVM for three-phase voltage source converters can give a quasi-optimal switching pattern, the stress and losses in switching devices are reduced, and the line current waveform is also improved. This control scheme is similar to the voltage oriented control, which uses PI controls in the synchronous rotating frame, and the SVM is employed to generate the desired output voltage vector in dq reference frame (Zhang et al., 2009). In (Benadli et al., 2015) sliding mode control is proposed for controlling VSC through tracking active and reactive power along predefined trajectories using integral sliding surface in the dq reference. Finally, it is important to mention the trend of using multilevel inverters because of the reduction of the distortion, less common voltage, less stress and the improvement of the power quality (Delavari et al., 2016; Desai and Shah, 2013), nevertheless the later is not applied in commercial applications because of the cost of including more power electronic devices in the PV system.

However, commercial applications usually use two-level VSC inverters and voltage oriented control with PI regulators because they provide a balance of complexity, capability, and economics. On the other hand, this control strategy does not include power quality functions such as voltage/reactive power control, harmonic compensations, and frequency/active power control, wasting the capacity of power converters for improving the power quality of distribution systems. Conventional control of VSC and most used in process control applications of PV systems will be presented in detail in chapter 2, while control strategies for including power quality functions will be proposed in chapters 3, 4, and 5.

1.2.2 Voltage and reactive power in photovoltaic systems

Solar energy is an ideal green energy for sustainable development strategy, it has special deductions on income tax, it has a long lifespan and, thanks to the resources of research centers, countries, and companies, its costs have been reduced by 70% in the last years, so that the penetration of solar energy into distribution electric systems has grown exponentially. Particularly, Colombia has approved the law 1715 of 2014 and the resolution 030-2018 of the National commission of gas and energy (*Comisión de regulación de energía y gas* CREG) to incentive renewable energy projects that have mainly increased the installation of PV generation in distribution systems. This new scenario makes it necessary to take into account the reactive power that is no longer generated because traditional systems will eventually be replaced by photovoltaic generation systems, which usually do not generate reactive power. Therefore, this new scenery could cause effects on the electric power systems such as voltage rise, reverse power flows, and inadequate protection and control systems. To face this new scenario, coordinated reactive power control studies for the regulation of the distribution network voltage with PV systems (Moondee and Shah, 2019), reactive power control methods for over voltage prevention (Demirok et al., 2011) and advanced protection (Li et al., 2011; Dwi et al., 2019) are proposed.

Intending to avoid voltage fluctuations and reverse power flows mentioned previously, among other issues related to the protection and control of distribution systems, Colombian regulation through the resolution 030-2018 of CREG (CREG-030-2018, 2018) limits the capacity of small-scale self-generation and distributed generation installation to 15% of the capacity of the circuit, transformer, or distribution substation, and usually limits the energy delivered to the grid to 50% of the average annual hours of minimum daily energy demand depending on the class of system generation, which is explained in detail in appendix C.4. Additionally, Colombian regulation through resolution 108-1997 of CREG (CREG-108-1997, 1997) established the criteria for reactive power control in the electric power service, however, in this resolution, only inductive reactive energy in electrical installations with the power factor greater than 0.9 was penalized, nevertheless, in the current method of remuneration for the distribution of electrical energy (CREG-015-2018, 2018) the capacitive reactive power penalty was introduced and a penalty variable M was included that varies between 1 and 12 depending on the frequency in that the user violates the regulatory limits of the power factor, this can be seen in detail in Appendix C.3.

1.2.3 Inertia emulation in photovoltaic systems

Synchronous generators play an important role in power systems because of their special attributes of inertia and their response under disturbances such as faults, loss of generators, and connection/disconnection of important loads (Anderson, 1995). More specifically, the intrinsic kinetic energy (rotor inertia) and the damping property (due to mechanical friction and electrical losses in the stator, the field, and the windings of the shock absorber) in synchronous machines allows smooth changes of the frequency (Ezequiel, 2016).

The integration of a large amount of built-in PV systems and distributed generation will have far-reaching consequences not only in the distribution networks, but also in the transmission and generation systems. If the PV generators are built on the roof and sides of the buildings, they will have the advantage of being located in urban areas and being electrically close to the loads, however, these PV power generating units may be subject to failures that can cause rapid and sudden disconnection of a large proportion of the power operation capacity, moreover, the distributed generation systems have a very small or null rotating mass, and by increasing the level of penetration of distributed resources, the impact of low inertia and the damping effect on dynamic performance and network stability increases, causing voltage/frequency fluctuations, making the system vulnerable to blackouts due to the lost of generators or important loads, and increasing failures in power systems, and therefore introduce challenges in terms of stability, reliability, power quality, and operation of power electric systems. Besides, it is important to mention that the reverse power of PV generation systems (Koyanagi et al., 2011) and the excessive supply of electricity in the network due to the total generation by the distributed generators can cause power fluctuations, the deterioration of the elements of the systems, the degradation of the power quality of the power electric system and fluctuations of frequency and voltage.

Conventional solar PV systems are integrated through power electronics converters which react differently compared to synchronous machines. One solution to this situation is to provide virtual inertia, which can be established for distributed generators and renewable generation systems using short-term energy storage together with a power electronics converter and appropriate control mechanisms to emulate the behavior of synchronous generators. This concept, known as virtual synchronous generator (VSG), allows the PV units to exhibit the inertia and damping properties of conventional synchronous machines for a short time (van Wesenbeeck et al., 2009). VSGs can provide a basis for integrating large amounts of PV systems whiteout jeopardize the stability of the grid, for that reason different schemes of virtual synchronous machines are proposed (Bevrani et al., 2013): VSYNC research group's VSG topology, the institute of electrical power engineering's topology, Osaka University ISE lab's VSG topology and Kawasaki Heavy Industries team research's topology is the mos recognized typologies.

1.2.4 Model predictive control

Model predictive control (MPC) is an optimization-based control method that has demonstrated to be efficient in industrial applications (Vargas, 2007). Being an optimization problem, MPC was initially applied to chemical process with slow dynamics (Dragicevic et al., 2017). Advances in computation capabilities have allowed to implement MPC in power systems applications and power electronics.

The main feature of MPC is the use of time horizons to be optimized but implementing only the current time slot. This allows us to anticipate future events and take control actions considering restrictions such as input limitations (usually due to actuator saturation), desired ranges of states and outputs, and desired performance specifications through weights in tracking errors and actuator efforts for the configuration of the control problem.

There are different versions of model predictive control, however, continuous MPC and FCS-MPC are the most common approaches for power electronics applications and they are the MPC applied in this thesis. Model predictive control has become a popular strategy for the control of power converters in recent years. In (Dragicevic et al., 2017) it is proposed to use a discrete model of the VSC with an associated filter to predict its future behavior for all possible control inputs and, consequently, apply the one that minimizes a programmed cost function (CF) in each time of sampling. The model predictive control has several advantages: MPC schemes are very simple, intuitive, and easy to implement, non-linearities and restrictions can be included in the model and multivariable and multi-objective optimization could be considered. In (Geyer, 2011) a comparison between conventional control schemes based on modulation and model predictive control is presented, and (Cortes et al., 2008) review the most important types of model predictive control applied in power electronics and drives.

The disadvantage of conventional MPC is the heavy computational load for the optimization and high calculations that can be made compared with to the conventional control, and especially represents a challenge in the inner loop where the dynamic is faster than the dynamic of the outer loop and, taking into account that there is a vast literature and industrial experience about how to deal with these concerns in the classical inner loop approach, we proposed to apply conventional model predictive control in the outer loop of the vector control (Useche et al., 2019) and as a complement of the control strategy for compensating harmonics show in Chapter 4.

Differently, FCS-MPC takes advantage of the limited number of switching states of the power converter for computing the optimal configuration of the voltage source converter in each step of the discrete model. This approach does not need modulation nor synchronization systems, it is flexible, easy to implement and it has a fast dynamic response (Panten et al., 2015). This last characteristic of the FCS-MPC is the reason why it is applied in this thesis for including the function of harmonics compensation, where it is necessary a fast response of the control system so that the inner loop is replaced by the FCS and the outer loop is calculated with a linear MPC that modifies the conventional control objectives of PV systems, which is explained in Chapter 4.

1.3 Scope and contribution of this thesis

This thesis explores different model predictive control approaches applied on power electronics converters, the requirements and concerns of power quality in distribution systems and proposed control strategies of photovoltaic and energy storage systems for improving power quality indexes. The contributions of the systems are as follows:

Improving voltage profile: Classic control is modified using model predictive control (MPC) for the outer loop and conventional vector oriented control for the inner loop, and it is applied a strategy for controlling the voltage of the distribution system substation through the control of the reactive power. The control strategy is tested over a realistic weak distribution system based on a Colombian primary feeder with deficit of reactive power.

Harmonic compensation: A new hierarchical control is proposed in order to include the harmonic compensation function, where the inner loop is replaced by the finite control set model predictive control (FCS-MPC), the outer loop is calculated with a linear MPC for controlling the voltage of the dc-link and the reactive control of the system and reference currents are computed using optimization theory.

Virtual synchronous machine: The virtual synchronous machine concept is applied through controlling of the active power of the energy storage in the capacitor taking advantage of the $P - V^2$ relationship of the capacitor of the dc-link of the voltage source converter, using the energy storage on the battery systems and applying model predictive control.

As a result of this thesis, a conference paper was presented in the 2019 International Conference on Smart Energy Systems and Technologies (SEST2019) in Porto-Portugal (Useche et al., 2019).

1.4 Outline of the document

This document is organized as follows: In Chapter 2 it is presented the main aspects of conventional vector oriented control for three-phase converters, including the subsystems required such as the synchronization system with the grid, the pulse width modulation, the Park/Clark transformation and the structure of cascade PI controls. Chapter 3 presents the theory of model predictive control (MPC) and its application on photovoltaic and storage systems, making modifications to the classic control to achieve conventional objectives and include control objectives related to the voltage performance of the grid. Chapter 4 reviews the concept of finite control set(FCS-MPC), its advantages, and the applications to voltage source converters (VSC). Also, it is presented the control of the dc-link using conventional PI control and MPC as well as FCS-MPC and optimization theory for harmonics compensation. Chapter 5 reviews the concept of the virtual synchronous machine and proposes a control strategy for improving the frequency response of a distribution system after a disturbance. Finally, the conclusions of the control strategies proposed for improving the power electric quality referent to voltage regulation, total harmonics distortion, and frequency control. Three appendices complement the thesis: Appendix A describes the synchronous reference frame using Park and Clarke transformation, the appendix B explains the main algorithms applied in the thesis and show some examples of model predictive control applications, and finally, Appendix C presents the Colombian regulation of power electric quality.

Chapter 2

Classic control of energy storage and photovoltaic systems

2.1 Average model of VSCs

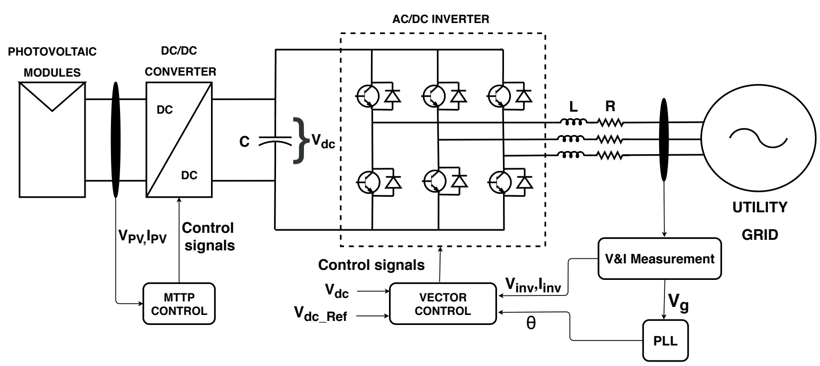

Figure 2.1: Classic photovoltaic system integrated with a voltage source converter

The classic configuration of a photovoltaic system is shown in Figure 2.1. It includes a photovoltaic panel, a dc/dc converter controlled by a maximum power point tracking (MMTTP) strategy, a two-level voltage-source converter (VSC) controlled by the conventional vector control, a capacitor on the dc side of the VSC and an LC filter on the side of the network. The current sensors are located at the terminals of the converter; these currents are transformed into a 0dq-reference frame (R.Teodorescu et al., 2011) using the voltage invariant transformation (see appendix A). The model of the VSC in 0dq-reference frame is show in Figure 2.2, where the voltage of grid is represented as a voltage source V_{grid} and the ac source V_{VSC} is the converter output voltage located just next to the semiconductors; the dc side of the converter is represented with a constant current source of magnitude I_{dc} in parallel with a capacitor C (Mulugeta, 2012).

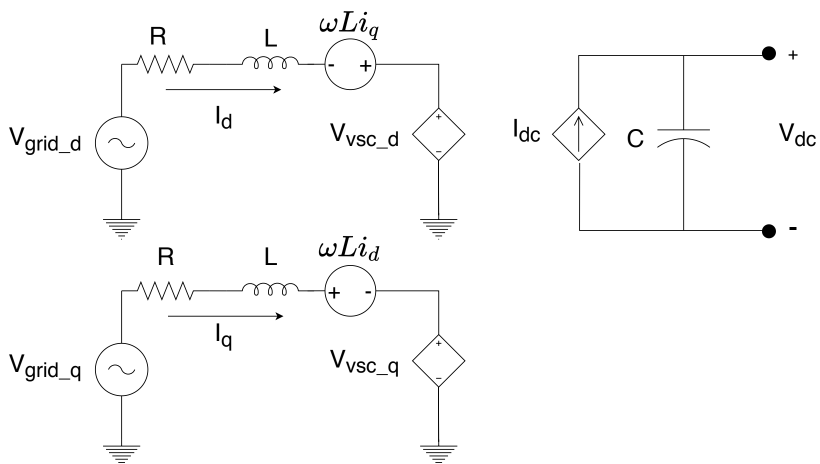

Figure 2.2: Model of the VSC using the synchronously rotating $0dq-$reference frame

Applying Kirchhoff's voltage law in the circuits of Figure 2.2 and making some algebraic reductions, the mathematical model of the VSC is obtained as given in (2.1):

$$L\frac{d}{dt}\begin{bmatrix} i_d \\ i_q \end{bmatrix} = \begin{bmatrix} V_{\text{grid\_}d} \\ V_{\text{grid\_}q} \end{bmatrix} \begin{bmatrix} V_{vsc\_d} \\ V_{vsc\_q} \end{bmatrix} - R.\begin{bmatrix} i_d \\ i_q \end{bmatrix} - \omega L \begin{bmatrix} 0 & 1 \\ -1 & 0 \end{bmatrix} \begin{bmatrix} i_d \\ i_q \end{bmatrix} \tag{2.1}$$

The dc side of the photovoltaic system consists on a solar panel integrated through a dc/dc converter for maximum power extraction. The vector control or voltage oriented control regulate the voltage of the dc-link and the reactive power as presented in the next section.

2.2 Vector oriented control

The objective of the vector control is to regulate the reactive power and the voltage of the dc-link. The basic principle is to control independently the components i_d and i_q of the currents in a 0dq-reference frame. The value of the angle θ required to sincronize the converter to the grid, is calculated by a phase-locked loop (PLL) (Bajracharya., 2008). The vector control scheme is shown in Figure 2.3. Each sub component is described below.

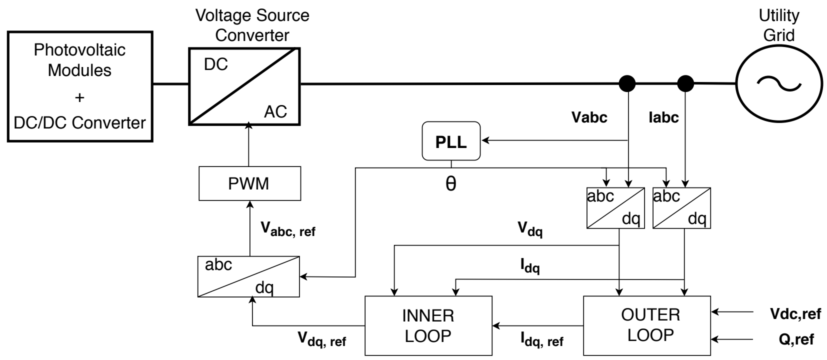

Figure 2.3: Vector oriented control

2.2.1 Network synchronization

A very important and necessary feature of VSC control is the network synchronization. This is done by the phase locked loop (PLL) which is able to detect the phase angle of the network voltage. The inputs of the PLL are the voltages measured on the side of the network and the output is the tracked phase angle θ and the frequency. The control of the PLL is done by adjusting the voltage of the axis q to zero; a PI controller is used for this purpose. By integrating the sum between the PI output and the reference frequency, the phase angle θ is obtained. Figure 2.4 depicts the classic PLL.

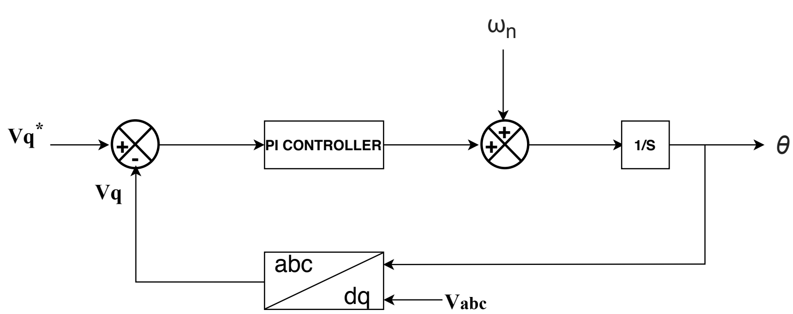

Figure 2.4: Structure of the Phase Lock Loop

2.2.2 Pulse width modulation

Pulse width modulation (PWM) aims to create trains of switched pulses which have the same fundamental volt-second average (i.e., the integral of the voltage waveform over time) as a target reference waveform at any instant. The major difficulty with these trains of switched pulses is that they also contain unwanted harmonic components which should be minimized. Hence for any PWM scheme, a primary objective can be identified which is to calculate the converter switch ON times which create the desired (low-frequency) target output voltage or current. Having satisfied this primary objective, the secondary objective for a PWM strategy is to determine the most effective way of arranging the switching processes to minimize unwanted harmonic distortion, switching losses, or any other specified performance criterion (Holmes and Lipo, 2003).

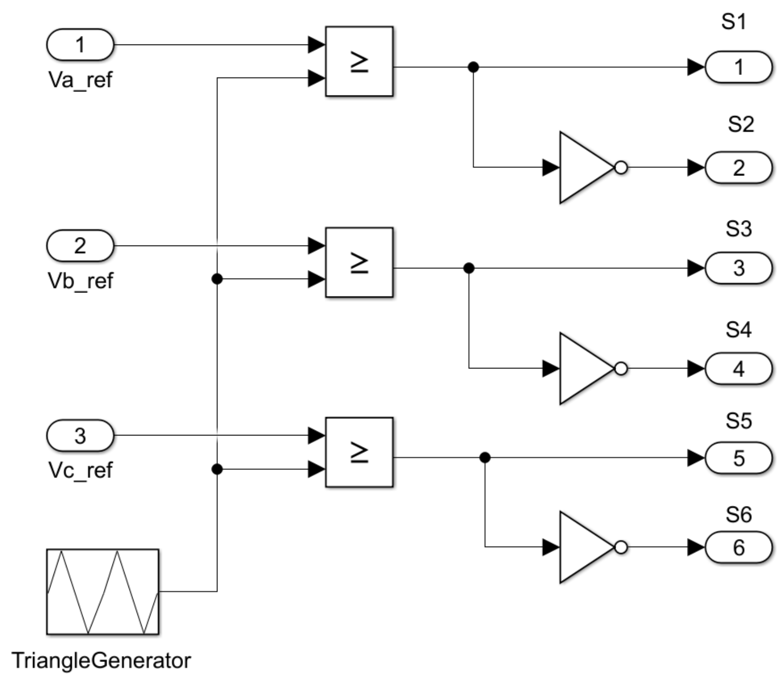

Figure 2.5: PWM implementation in SIMULINK/MATLAB

2.2.3 Per unit representation

There are different ways to represent the system in per unit. Usually, the base values are chosen to fit a voltage invariant transformation. S_{base} represents the nominal three phase power of the system and V_{base} the peak value of the rated ac voltage of the system with the following equation:

$$V_{\text{base}} = \frac{2}{3} V_{LL,rms} \tag{2.2}$$

Where $V_{LL,rms}$ is the rms value of the line voltage. The basis for the unit transformation is chosen to achieve an invariant power transformation, so that the power of the ac and dc sides is the same, therefore,

$$I_{\text{base}} = \frac{2}{3}\frac{S_{\text{base}}}{V_{\text{base}}} \tag{2.3}$$

The power balance is given by the next equation:

$$S_{\text{b}} = \frac{3}{2}V_{\text{base}}I_{\text{base}} = V_{\text{dc-base}}I_{\text{dc-base}} \tag{2.4}$$

The base of the dc-link is the minimal voltage required for avoiding over modulation as follows (R.Teodorescu et al., 2011):

$$V_{\text{dc-base}} = 2V_{\text{base}} \tag{2.5}$$

The base of the dc current is presented below:

$$I_{\text{dc-base}} = \frac{3}{4}I_{base} \tag{2.6}$$

While the basis of the system impedance is defined as:

$$Z_{dc,base} = \frac{V_{dc,base}}{I_{dc,base}} = \frac{8}{3}Z_b \tag{2.7}$$

2.2.4 Inner control loop

The inner control loop takes as input the error between the reference current and the measured current. This error is transmitted through the PI control and the decoupling terms are compensated by the feed forward. As a result, the desired converter voltage is obtained the reference frame dq. The structure of the inner loop is presented in Figure 2.6, notice that two PI regulators are required for the axes q and d respectively (Kalitjuka, 2011).

2.2.5 Outer loop

Active and reactive power are given by (2.9) in per unit representation.

$$p = v_d i_d + v_q i_q \tag{2.8}$$
$$q = v_d i_q - v_q i_d \tag{2.9}$$

However, since $v_q = 0$ and v_d is assumed constant, then active power is proportional to i_d whereas reactive power is proportional to i_q. This is the principle of the outer loop which allows to control of active power through the converter, reactive power at each side of the VSC and/or dc-link voltage (Kalitjuka, 2011). Current i_d is used to control the active power whereas current i_q is used to control the reactive power. It is also possible to control the voltage on the dc-link using the current i_d as shown in Figure 2.7

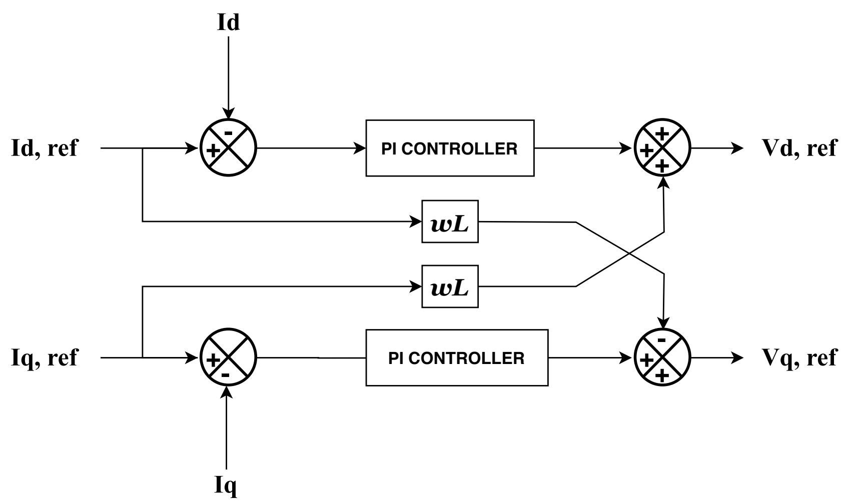

Figure 2.6: Structure of the inner current controller

2.3 Energy storage system

The battery energy storage system (BESS) models used in this document mainly include a bidirectional dc/dc , a dc-link capacitor, a three-phase bidirectional ac/dc converter, an ac filter and a transformer that connect the system to the electrical network. In this section, these models and the corresponding parameters are discussed, and the control techniques are also described.

Figure 2.8 shows in detail the components of a BESS. The bidirectional dc/dc converter is used to control the voltage of the dc-link capacitor by charging and discharging the battery. The inverter uses a cascaded PI controller to generate

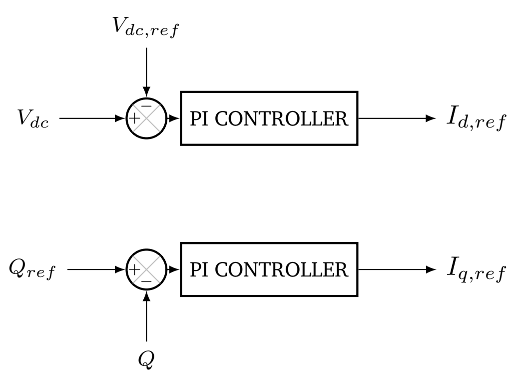

Figure 2.7: Block diagram of the outer loop

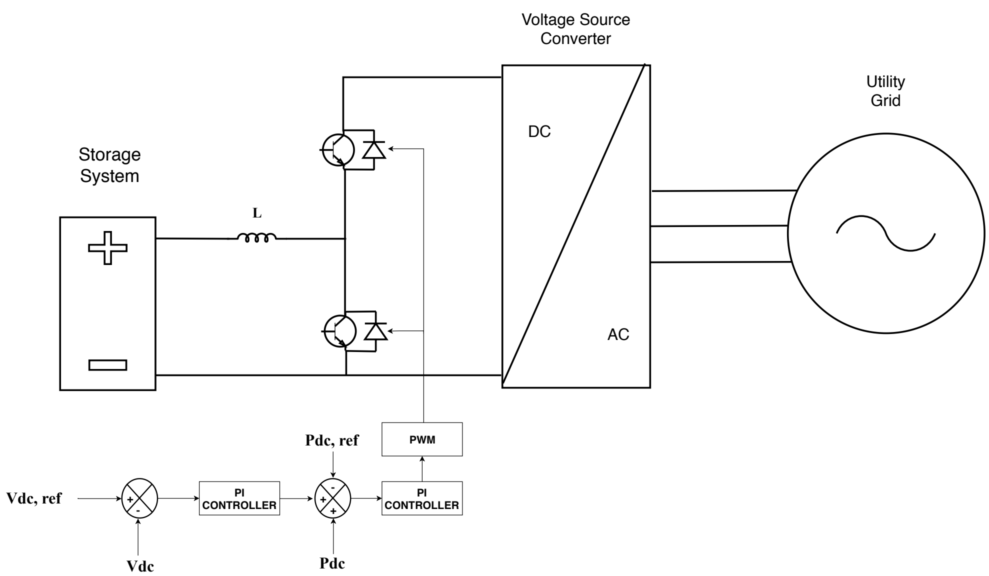

Figure 2.8: Energy storage system

the duty cycle for the switches according to the difference of the dc-link voltage and its reference, as shown in Figure 2.8. It is important to keep in mind that the second PI controller reacts to changes in the active power of the first system, which improves the capacity of the bidirectional dc/dc controller to regulate the dc-link voltage. When the dc link voltage is lower than the predefined set point, the inverter operates in boost mode, discharging the battery. When the dc-link voltage is greater than the set point, the converter works in buck mode, charging the battery (Farrokhabadi et al., 2018). In Figure 2.8 is illustrated how the dc/ac converter connects the battery and the bidirectional dc/dc converter to the network through the ac filter.

2.4 Results of the classic control of photovoltaic systems

The vector control was implemented over a energy storage and photovoltaic system with the parameters of the table 2.1, which is based on a realistic system. In addition, the parameters of the PI controller are shown in tables 2.2 and 2.3, which were heuristically calculated.

The results are shown in Figures 2.9 and 2.10. In Figure 2.9 it is shown the results of the voltage control of the dc-link, showing a slow behavior and important fluctuations around the reference of the voltage of the dc-link. Specifically, the results show that the PI controller has an settling time of 0.251 seconds, an

	L	C	R
VSC	2.5 mH	50 μF	0.08 Ω
DC/DC converter	10 mH	NA	NA

Table 2.1: Parameters of the energy storage and photovoltaic system

	P	I
Inner loop	1	300
Outer loop	200	10000

Table 2.2: Outer loop PI control parameters

undershoot of 21%, and an overshoot of 15.58%.

On the other hand, Figure 2.10 presents the results of the control of the reactive power, showing a faster response and lower fluctuations with respect of the control of the voltage of the dc-link, however, the overshoot of the reactive control is higher than the control of the voltage of dc-link. Concretely, the results show a settling time of 0.17 seconds and an overshoot of 24.9%.

	P	I
Voltage control	1	300
Power control	200	10000

Table 2.3: DC/DC converter PI control parameters

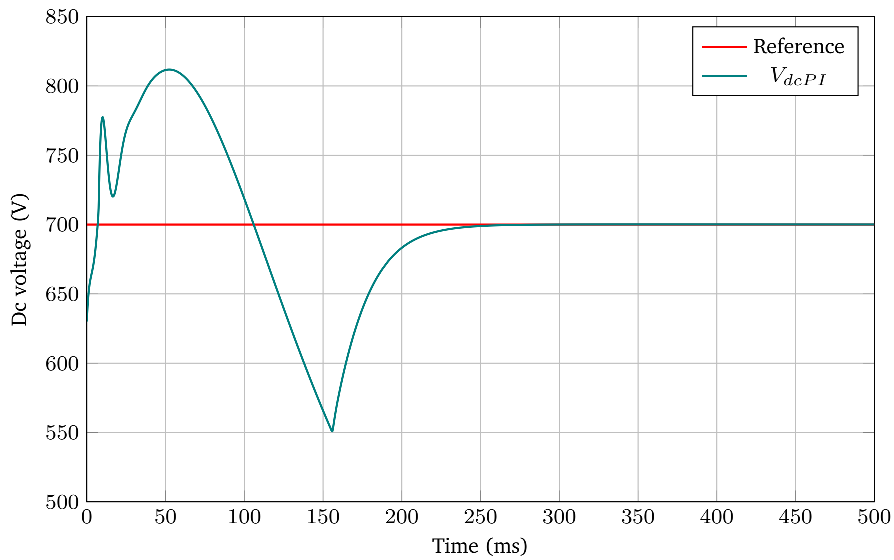

Figure 2.9: Voltage control results of the dc link

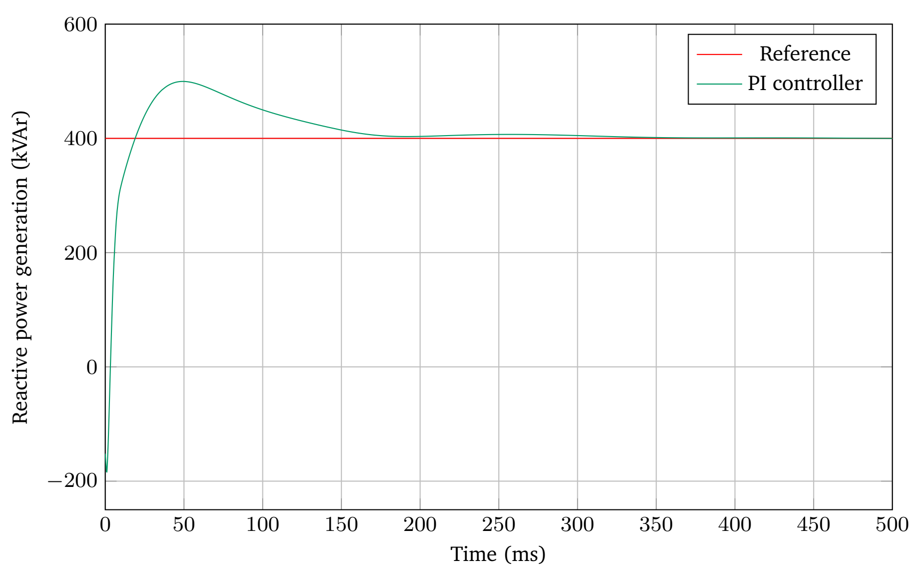

Figure 2.10: Reactive control results

Chapter 3

Control of energy storage and photovoltaic systems using model predictive control

3.1 Model predictive control

The theory of predictive control based on the model is a control technique that is being researched and applied widely and successfully in industrial processes due to its flexibility, precision and inherently fast response (Dragicevic et al., 2017). The main advantage of model predictive control (MPC) based on the model is the fact that it optimizes present and immediate future time horizons, while also taking into account future time horizons. This is achieved by optimizing a finite time horizon, but implementing only the current time slot, which allows us to anticipate future events and take control actions consequently by means of the process model, restrictions on system variables, such as limitations input (usually due to actuator saturation), desired ranges of states and outputs, and desired performance specifications through different weights in tracking errors and actuator efforts for the configuration of the control problem.

3.1.1 State space system

The predictive control uses the model of the plant to make predictions of the future results of a process, whereby, the model of the plant plays a fundamental role in its operation. In the present work the plant of the system will be modeled by means of a model in space of states of the following form:

$$\begin{aligned} x_m(k+1) &= A_m x(k) + B_m u(k) \\ y(k) &= C_m x(k) + D_m u(k) \end{aligned} \tag{3.1}$$

Where x is the vector of system states, u is the vector of system inputs and y is the vector of system outputs. However, due to the principle of "recending horizon", where current plant information is required for prediction and control, it is implicitly assumed that the input $u(k)$ does not affect the output $y(k)$ in the same sampling time. That is, D_m is a matrix of zeros of dimension $q \times p$ in the model of the plant.

Additionally, the system must be discretized to apply predictive control. It is common in digital control for the converter to be built so that it holds the analog signal constant until a new conversion is ordered. This is called a zero order hold circuit.

The sampling times t_k are chosen as the moments at which the control changes. Since the control signal is discontinuous, it is necessary to specify its behavior in the discontinuities. The convention is adopted that the signal is continuous on the right. Thus, the control signal is represented by the sampled signal $u(t_k) : k = \ldots, -2, -1, 0, 1, 2, \ldots N$. The relationship between the variables of the system at the time of sampling will be determined. So the state in t where $t_k \leq t \leq t_{k+1}$ is:

$$
\begin{aligned}
x(t) &= e^{At(t-t_k)}x(t_k) + \int_{t_k}^{t} e^{A(t-s')}Bu(s')ds' \\
&= e^{A(t-t_k)}x(t_k) + \int_{t_k}^{t} e^{A(t-s')}ds'Bu(t_k) \\
&= e^{A(t-t_k)}x(t_k) + \int_{0}^{t-t_k} e^{As}dsBu(t_k) \\
&= \Phi(t,t_k)x(t_k) + \Gamma(t,t_k)u(t_k)
\end{aligned}
$$

Where it has been taken into account that $u(t_k)$ is constant between the sampling times and the change of variable $s' = t - s$ was made . The state vector at t is thus a linear function of $x(t_k)$ and $u(t_k)$. If the D/A and A/D converters are perfectly negligible, it can be considered that the input u and the output y are sampled at the same time. Thus, the behavior of the system at the sampling times is described by:

$$
\begin{aligned}
x(t_{k+1}) &= \Phi(t_{k+1},t)x(t_k) + \Gamma(t_{k+1},t)u(t_k) \\
y(t_k) &= Cx(t_k) + Du(t_k)
\end{aligned}
$$

Where:

$$
\begin{aligned}
\Phi(t_{k+1},t_k) &= e^{A(t_{k+1}-t_k)} \\
\Gamma(t_{k+1},t_k) &= \int_{0}^{t_{k+1}-t_k} e^{As}dsB
\end{aligned}
$$

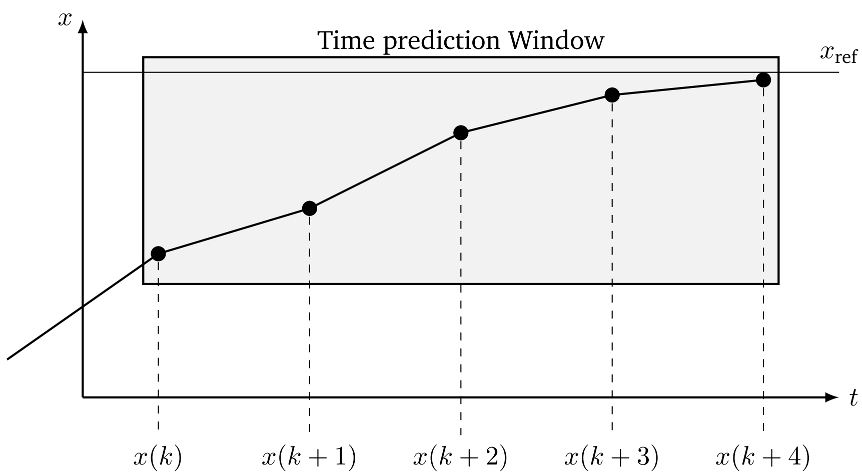

Figure 3.1: Time window applied in model predictive control

Although MPC has been used before for the control of power electronics converters, these applications consider a discrete framework with one step of prediction. In contradistinction with that approach, this thesis proposes to apply MPC with a time window with several steps for the outer loop as shown in Figure 3.1.

The objective of the control is to make the output vector y reaches the desired value y_{ref} (Wang, 2008). The concept of receding horizon is used by applying the control action $u(k)$ and resolving the optimization problem again for the time $k + 1$. In general, the problem can be represented in a finite horizon as presented below:

$$\begin{aligned} x(k+1) &= Ax(k) + Bu(k) \\ x(k+2) &= Ax(k+1) + Bu(k+1) \\ &\vdots \\ x(k+N) &= Ax(k+N-1) + Bu(k+N-1) \end{aligned} \tag{3.2}$$

By replacing the state vector sequentially, and organizing in a matrix form it can be aimed:

$$\begin{bmatrix} x(k+1) \\ x(k+2) \\ \vdots \\ x(k+N) \end{bmatrix} = \begin{bmatrix} A \\ A^2 \\ \vdots \\ A^N \end{bmatrix} x(k) + \begin{bmatrix} B & 0 & \dots & 0 \\ AB & B & \dots & 0 \\ \vdots & \vdots & \vdots & \\ A^{N-1}B & A^{N-2}B & \dots & B \end{bmatrix} \begin{bmatrix} u(k+1) \\ u(k+2) \\ \vdots \\ u(k+N) \end{bmatrix} \tag{3.3}$$

With the previous matrix equation, the outputs y and the inputs u are related as in the next way:

$$\begin{bmatrix} y(k+1) \\ y(k+2) \\ y(k+3) \\ \vdots \\ y(k+N) \end{bmatrix} = \begin{bmatrix} CA \\ CA^2 \\ CA^3 \\ \vdots \\ CA^N \end{bmatrix} x(k) + \begin{bmatrix} CB & 0 & \dots & 0 \\ CAB & CB & \dots & 0 \\ \vdots & \vdots & \vdots & \vdots \\ CA^{N-1}B & C * A^{N-2}B & \dots & CB \end{bmatrix} \begin{bmatrix} u(k+1) \\ u(k+2) \\ \vdots \\ u(k+N) \end{bmatrix}$$

Which can be written compactly as follows:

$$Y = FX_m + GU \tag{3.4}$$

Where:

$$Y = \begin{bmatrix} y(k+1) \\ y(k+2) \\ \vdots \\ y(k+N) \end{bmatrix}, \; U = \begin{bmatrix} u(k+1) \\ u(k+2) \\ \vdots \\ u(k+N) \end{bmatrix}, \; F = \begin{bmatrix} CA \\ CA^2 \\ \vdots \\ CA^N \end{bmatrix}$$
$$G = \begin{bmatrix} CB & 0 & \dots & 0 \\ CAB & CB & \dots & 0 \\ \vdots & \vdots & \vdots & \vdots \\ CA^{N-1}B & CA^{N-2}B & \dots & CB \end{bmatrix}$$

And X_m are the states measured in the current iteration. Defining the reference matrix $R = [y_{\text{ref}}(k+1),\ y_{\text{ref}}(k+2), \dots y_{\text{ref}}(k+N)]$ and $W = [u_{\text{ref}}(k+1), u_{\text{ref}}(k+2), \dots u_{\text{ref}}(k+N)]$, the optimization problem can be formulated in the following way:

$$\begin{aligned} \min\ J(k) &= \frac{1}{2}(R-Y)^\top(R-Y) + \frac{1}{2}(U-W)^\top Q(U-W) \\ \text{subjet to: } & Y = FX_m + GU \end{aligned} \tag{3.5}$$

To solve this optimization problem, the following Lagrangian is proposed:

$$\begin{aligned} \mathcal{L}(Y,U,\lambda) =& \frac{1}{2}(R-Y)^\top(R-Y) + \frac{1}{2}(U-W)^\top Q(U-W) \\ & - \lambda^\top(FX_m + GU) \end{aligned} \tag{3.6}$$

Applying the conditions of optimally and solving the resulting equation system, it can be obtained the optimal output matrix:

$$U = (G^\top G + Q)^{-1}(QW + G^\top R - G^\top FX_m) \tag{3.7}$$

3.2 Outer-loop using model predictive control

This section proposes to apply model predictive control for the outer loop, which in comparison of classical PI controller is more efficient because the MPC could be considered an optimal control in real time. In addition, the use of MPC for power electronic converters is usually based on one step in the modulation, but our proposal includes a larger time horizon allowing a more efficiently and faster performance. A VSC converter contains a dc-link voltage controller that influences the stability of the system and that must be included in the simulations. The dc-link voltage controller acts as a filter of the power that is injected into the network, so that it is invariant in time. Making a balance of powers, the following expressions are obtained:

$$P_{dc} = P_{ac} + P_{capacitor} \tag{3.8}$$

$$v_{dc}i_0 = P_{ac} + CV_{dc}\frac{dV_{dc}}{dt} \tag{3.9}$$

$$P_0 = P_{ac} + CV_{dc}\frac{dV_{dc}}{dt} \tag{3.10}$$

Where P_0 is the generation power of the photovoltaic modules, P_{ac} is the power in the ac side of the VSC and P_{dc} is the power in the dc side of the VSC. Assuming there are no losses in the switching devices of the VSC and replacing the power balance, it is accomplished:

$$Cv_{dc}\frac{dv_{dc}}{dt} = P_0 - \frac{3}{2}v_d i_d \tag{3.11}$$

$$\frac{dv_{dc}}{dt} = \frac{1}{Cv_{dc}}(p_0 - \frac{3}{2}v_d i_d) \tag{3.12}$$

It is evident that this equation is non-linear, so a linearization is made around the operation point (*):

$$\frac{d(\Delta V_{DC})}{dt} = -\frac{1}{C(V_{dc}^*)^2}(P_0 - \frac{3}{2}v_d^* i_d^*)\Delta v_{dc} - \frac{3V_d}{2C(V_{dc}^*)}\Delta i_d \tag{3.13}$$

The representation can be modeled in the following way:

$$\dot{x} = Ax + Bu \tag{3.14}$$

$$y = Cx \tag{3.15}$$

Where:

$$
\begin{aligned}
&x = V_{dc}, u = i_d \; and \; y = V_{dc} && (3.16)\\
&A = -\frac{1}{C(V_{dc}^{*})^2}(P_0 - \frac{3}{2}V_d^{*}i_d^{*}) && (3.17)\\
&B = -\frac{3V_d^{*}}{2C(V_{dc}^{*})} && (3.18)\\
&C = 1 && (3.19)
\end{aligned}
$$

This model constitutes the state space of the outer loop and it is used to apply the MPC over the voltage source converter of the PV and energy storage system.

3.3 Control strategy of photovoltaic systems for improving Voltage Profiles

The reactive power could be controlled by the q component of the current (i_q) through the next equation:

$$Q = i_d V_q - i_q V_d \quad (3.20)$$

It is usually to set the reference of the q component of the current i_q as zero, however our objective is to inject reactive power in order to improve the voltage profile. Taking into account the previous reason, the voltage of the PV and the energy storage system is used for computing the reference of the i_q in order to control the voltage in the set substation voltage reference. In Figure 3.2 the complete control proposed is shown.

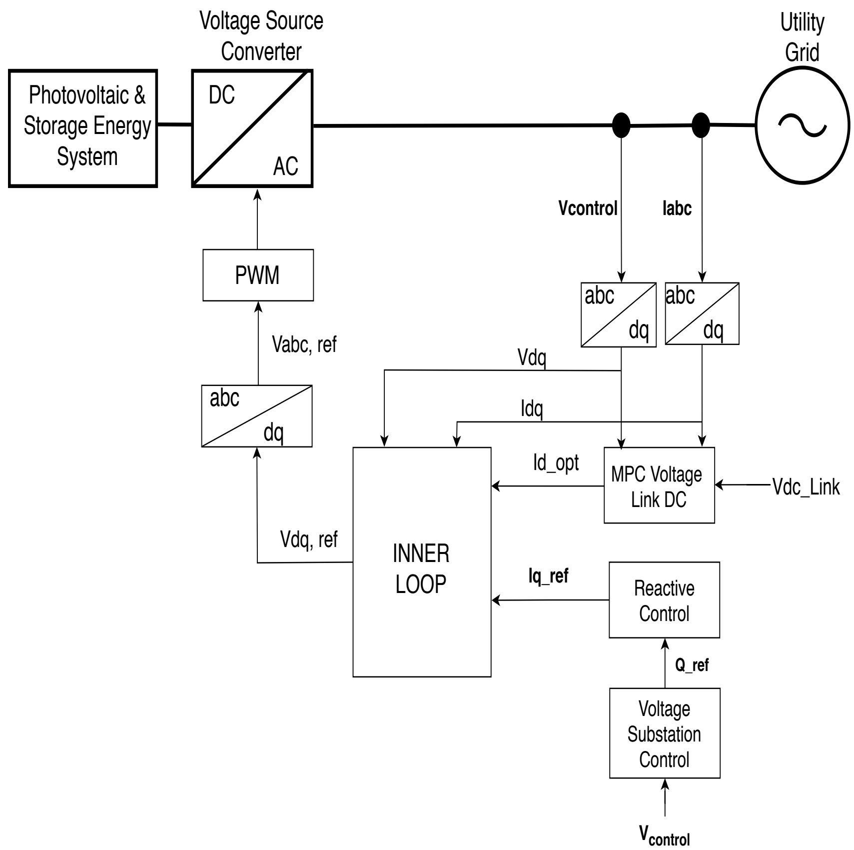

Figure 3.2: Control of the VSC using MPC and reactive control for improving the voltage profile

The regulation of the voltage profile is done by injecting reactive power to the grid. The reactive power injected to the grid depending on the difference between the reference voltage and the measured substation voltage so that for a very high error, the reactive power that is injected into the grid increases significantly until the error is lower than a predefined value, then the reactive power increases in lower quantities until the reference voltage is reached.

3.4 Results of the control of photovoltaic and energy systems for voltage regulation

The proposed control was simulated in Matlab/Simulink over the distribution power electric system prototype is shown in Figure 3.3, which is a realistic weak distribution system, based on a Colombian primary feeder with deficit of reactive power, a low short circuit power, low power factor loads and vulnerable to load variations that generate voltage variations and power quality phenomena in normal conditions. The battery energy storage system (BESS) models simulated in this document include a bidirectional dc/dc converter in parallel with the photovoltaic modules and connected to the power grid through a VSC, this configuration could see in Figure 3.4. The parameters of the energy storage and the photovoltaic system is presented in Table 3.1 and the reference voltage of the substation is set in 7200 V.

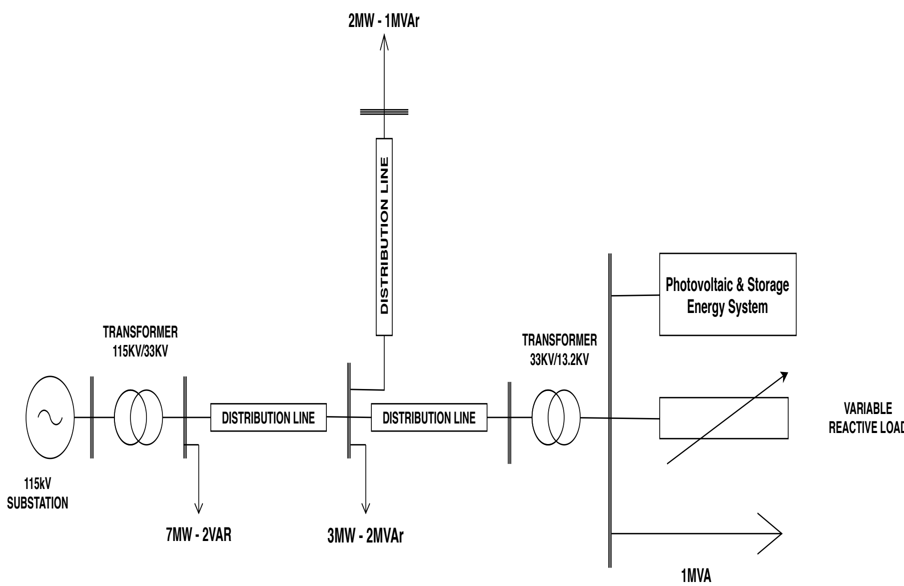

Figure 3.3: Electric distribution system prototype

PV system power	Storage system power	V_{dc}	V_{ac}
400kVA	100KVA	700V	400V

Table 3.1: Parameters of the photovoltaic and energy storage system

The implementation uses MPC with a time window of twenty steps ($N = 20$), and the reactive power control uses three different steps that depends on the error of the voltage profile in order to reach the reference of the voltage control in a shorter time and without significant variance in stationary time. The VSC has a nominal power value of 500 kVA, and the limit of the current is set as $I_{\text{max}} = 1.2 I_{\text{nom}}$ and this is the reference for the limit of the reactive power that the photovoltaic and the storage energy system can inject to the grid.

In Figure 4.7 is shown the results of the voltage control of the dc-link, showing that the PI controller has an settling time of 0.251 s, while the MPC of the dc-link has an settling time of 0.068 s, which means an improvement of 72.9%.

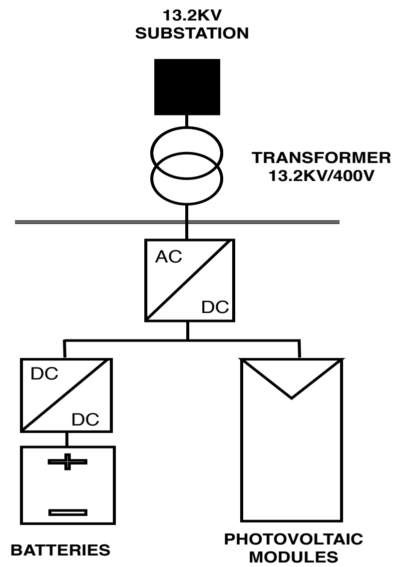

Figure 3.4: Energy storage system and photovoltaic system

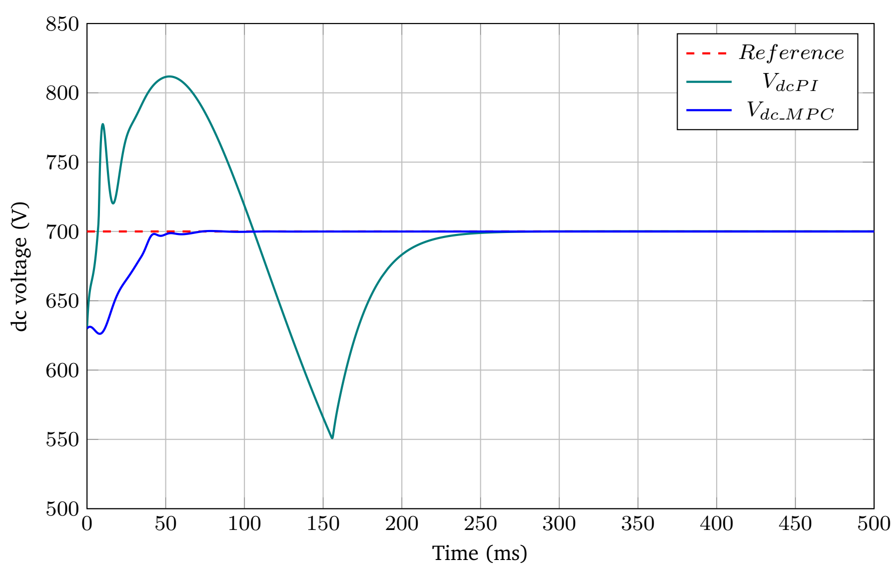

Figure 3.5: Voltage control results of the dc-link

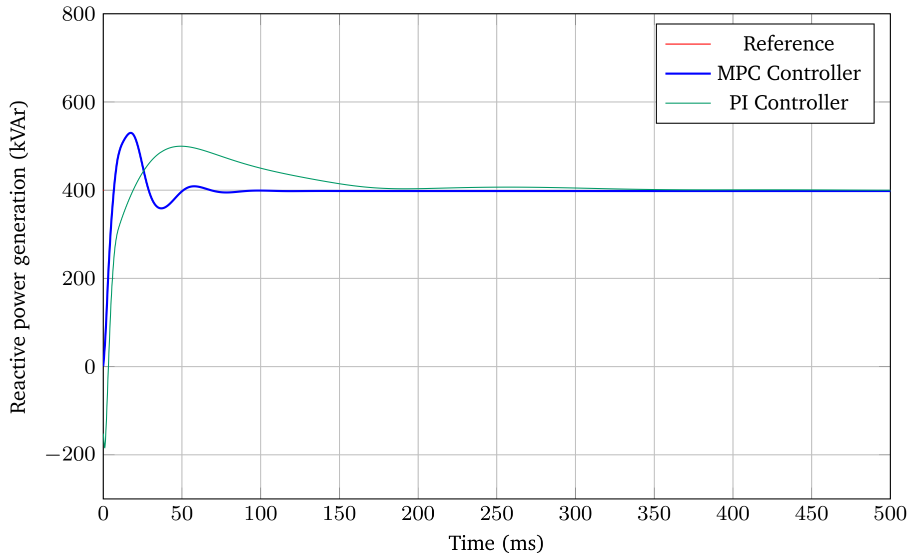

Figure 3.6: Reactive control results

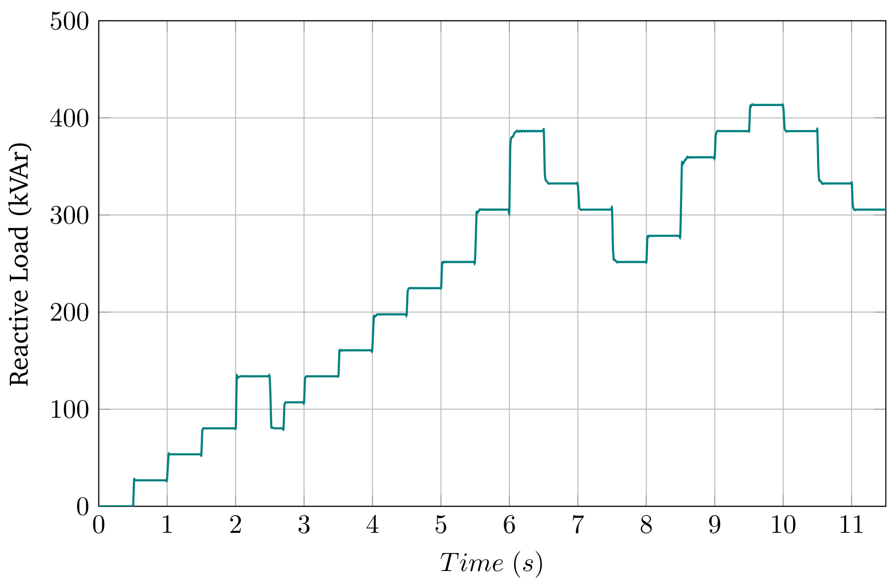

Figure 3.7: Reactive load

	Overshoot	Settling time
PI controller	15.58%	251 ms
MPC controller	0.0%	68 ms

Table 3.2: Results of the dc voltage Control

	Overshoot	Settling time
PI controller	24.9%	170 ms
MPC controller	32.4%	89 ms

Table 3.3: Results of the reactive control

Besides, the results of the PI control over the voltage of the dc-link show an overshoot of 15.58%, while the MPC does not present overshoot, and has fewer fluctuations.

On the other hand, Figure 4.8 shows the results of the control of the reactive power. From these results, we can conclude that the MPC has a faster response than the PI controller. Specifically, the PI controller presents an settling time of 0.170 s, while the MPC has an settling time of 0.089 s which means an improvement of 47.6%.

Finally, Figure 3.8 shows the control of the voltage profile of the substation of the photovoltaic and energy storage systems over the tested distribution system proposed. The results show that the voltage profile of the substation can be controlled through the reactive power generation of the photovoltaic and energy storage system with a time which helps to guarantee the Colombian limits of the steady state voltage.

.

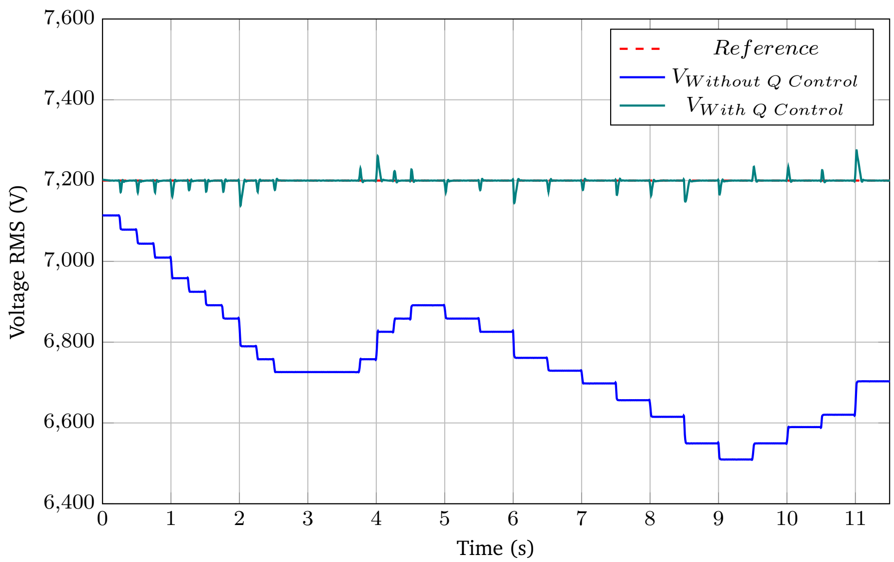

Figure 3.8: Results of the control of the substation voltage profile

Chapter 4

Finite control set model predictive control

Power electronics technologies have improved considerably the efficient of industrial and commercial processes, but the high penetration of this technology implies a reduction of the electric power quality, due to the high harmonic pollution generated by line-commutated converters. In addition, penetration of renewable energies into the power system affects the power quality of the system due to the commutation of power converters and the variability of primer energy sources such as solar or wind energy (Barutcu et al., 2020).

In this chapter the conventional control of photovoltaic systems is modified in order to include the function of harmonics compensation applying optimal conventional model predictive control (MPC), finite control set model predictive(FCS-MPC) and optimization theory to compensate harmonics of non-linear loads. The current of the VSC is control through the FCS-MPC that evaluate an objective function in order to select the configuration of the power switching devices that minimize the error between the current of the VSC and the reference currents. First PI regulator is used to control the voltage of the dc-link, and then the conventional MPC is proposed to regulate the voltage of the dc-link using a discrete frame and the concept of receding horizon through a large time window with multiple steps that allows to set an optimization problem that calculate the power of the capacitor that is needed for regulating the dc voltage of the VSC. Finally, the compensation of harmonics is control through an optimization problem that calculate the current reference of the VSC in order to inject the current that minimize the harmonics components of the grid.

4.1 Finite control set model predictive control for photovoltaic systems

Finite control set model predictive control (FCS-MPC) takes advantage of the finite states of the switches of a voltage source converter (VSC) in order to minimize an objective function that could be designed for controlling different variables such as voltage, current or power, and allows include constraints such as power factor approaches or physical limitations (Rodriguez et al., 2013). This thesis chapter is focused on the control of the current of the VSC using the $\alpha\beta$ reference frame. The concept of the FCS-MPC is shown in Figure 4.1.

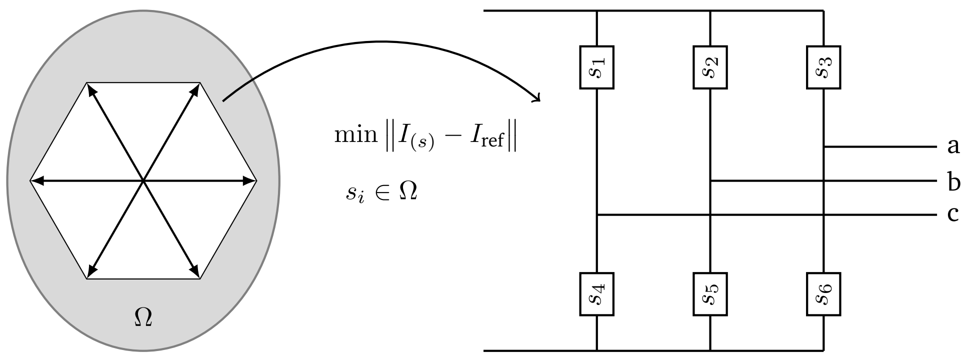

Figure 4.1: Concept of FCS

The set Ω consists of 8 possible switching configurations, when it turns, generates 8 possible output of currents. The main idea is to calculate future possible currents of the VSC through the measured variables of the VSC, evaluation of all possible switching states and selection of the switching state $s \in \Omega$ that minimize the cost function (T. and S.Mishra, 2018).

The prediction of the current can done by equation (4.1).

$$v_p(t) = Ri(t) + L\frac{di(t)}{dt} + v_g(t) \tag{4.1}$$

The control is formulated in discrete time, therefore equation (4.1) is discretized using Euler forward method to get equation (4.2) below:

$$i^p(k+1) = \left(1 - \frac{RT_s}{L}i(k) + \frac{T_s}{L}(v_p(k) - v_g(k))\right) \tag{4.2}$$

Where R and L are the resistance and inductance of the VSC, respectively; T_s is the sampling time, v_g is the voltage of the grid, $i(k)$ is the measured load current, and the inverter voltage $v_p(k)$ is the decision variable to be calculated by the controller and can get from the table 4.1.

The FCS-MPC algorithm contains five major steps that can be summarized as follows:

1. Measure the load currents.
2. Predict the load currents for the next sampling instant for all the possible switching states.
3. Evaluate the cost function for each prediction.
4. Select the switching state that minimizes the cost function.
5. Apply the new switching state.

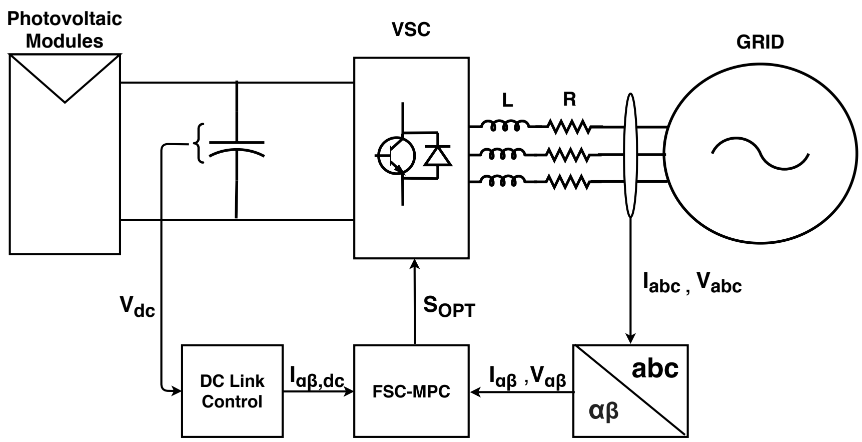

Figure 4.2: Control of a photovoltaic system using FCS

4.2 Control of the dc-link voltage of the VSC

4.2.1 dc-link voltage control using PI control

The control structure for the regulation of the voltage of the dc link using a PI controller is showing in Figure 4.3. In this strategy, the PI controller is used for computing the current reference of the capacitor (Podder and Habibullah, 2016), and then the capacitor power is calculating as $P_C = I_{\text{ref}} V_{dc}$.

4.2.2 Control of the dc-link voltage using model predictive control

This section shows the control of the voltage of the dc-link of the voltage source converter(VSC) using the model predictive control methodology presented in Chapter 3. For that reason, the plant of the system is modeled in the space-state representation shown in equation (3.1).

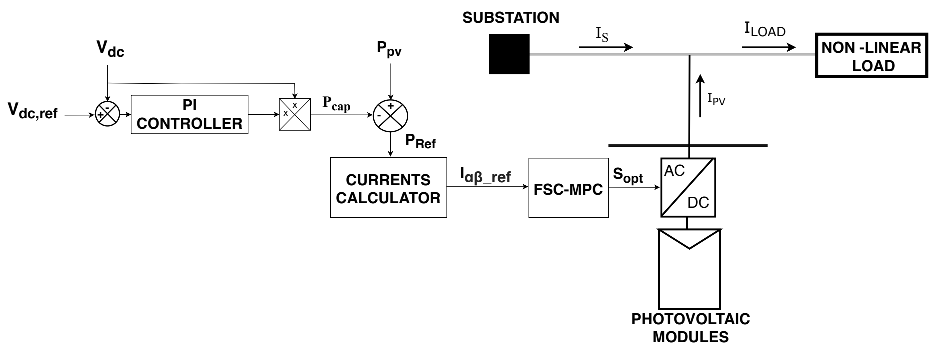

Figure 4.3: Control of dc-link Using PI controller

In order to obtain a space-state representation of the dc-link voltage, we use the concept of the energy of the capacitor by using its energy storage that can be calculated with equation (4.3).

$$E_C = \frac{1}{2} C.V_C^2 \tag{4.3}$$

It is important to remember that for the power of the capacitor it can be used the derivative of the energy in the discrete frame as shown in equation (4.4):

$$P_C = \frac{dE_C}{dt} = \frac{E_C(k+1) - E_C(k)}{Ts} \tag{4.4}$$

From (4.4), we can get the space-state model of the system by discretizing equation (4.4) through the Euler forward method, using a sample time T_s:

$$E_C(k+1) = E_C(k) + T_s.P_C(k) \tag{4.5}$$

$$y(k) = E_C(k) \tag{4.6}$$

Once the model in the state space of the dc-link is obtained, we can apply the MPC described in Chapter 3, taking into account that the output control signal is $y(k) = E_C(k)$ and the input control signal is the power injected to the capacitor $u(k) = P_C(k)$, and the idea is to inject power to the capacitor to store the necessary energy in the capacitor, which can be computed with (4.3), to reach the voltage reference as shown in Figure 4.4.

The structure of the control of the dc-link using MPC can see in Figure 4.5.

4.3 Control strategy for harmonics compensation

The idea of this proposed strategy is that the photovoltaic system injects the current I_{PV} for reducing the harmonics of the current of the source I_S with the restriction of the power generated by the photovoltaic panels (Garces et al.,

Voltage Vector	Voltage output	
V_0	$V_\alpha = 0$	$V_\beta = 0$
V_1	$V_\alpha = \frac{2}{3}V_{dc}$	$V_\beta = 0$
V_2	$V_\alpha = \frac{1}{3}V_{dc}$	$V_\beta = \frac{\sqrt{3}}{3}V_{dc}$
V_3	$V_\alpha = -\frac{2}{3}V_{dc}$	$V_\beta = \frac{\sqrt{3}}{3}V_{dc}$
V_4	$V_\alpha = -\frac{2}{3}V_{dc}$	$V_\beta = 0$
V_5	$V_\alpha = -\frac{1}{3}V_{dc}$	$V_\beta = -\frac{\sqrt{3}}{3}V_{dc}$
V_6	$V_\alpha = \frac{1}{3}V_{dc}$	$V_\beta = -\frac{\sqrt{3}}{3}V_{dc}$
V_7	$V_\alpha = 0$	$V_\beta = 0$

Table 4.1: Possible output voltages

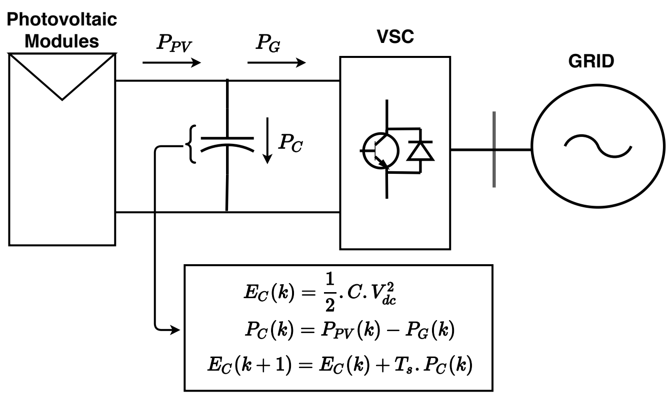

Figure 4.4: Strategy for controlling the voltage of the dc-link using MPC

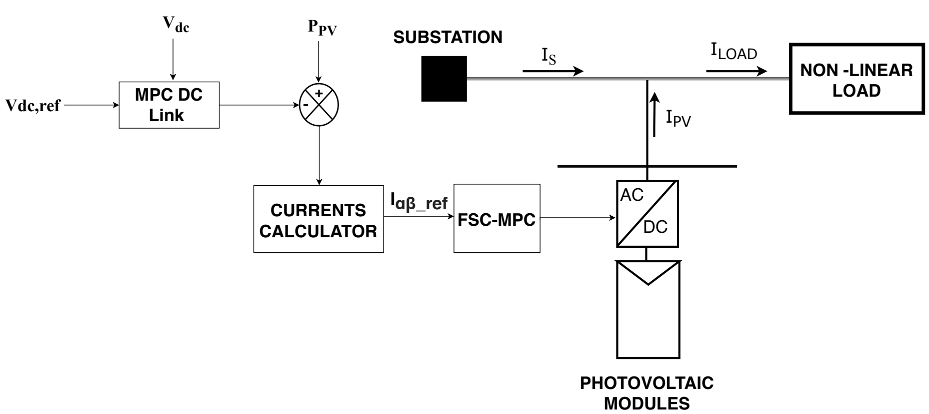

Figure 4.5: Control of dc-link using MPC

2012) in order to reduce the harmonics of the grid of the figure 4.6. With the objective to compensate harmonics using photovoltaic systems and taking into account the restriction of the power that the photovoltaic system can generate, this work proposes to resolve the mathematical optimization problem set in equation (4.7) to compute the optimal currents that the photovoltaic system must inject to the grid for reducing the harmonics that the source have to inject to the grid.

$$\begin{aligned} &\min \frac{1}{2}(I_{L_\alpha} - I_{P_\alpha})^2 + \frac{1}{2}(I_{L_\beta} - I_{P_\beta})^2 \\ &P_{PV} = V_\alpha I_{P\alpha} + V_\beta I_{P\beta} \end{aligned} \tag{4.7}$$

The previous optimization problem proposed in equation (4.7) can easily resolve using the method of Lagrange multipliers, where we can obtained the current references $I_{\alpha_{ref}}$ and $I_{\beta_{ref}}$ of the photovoltaic system through (4.8):

$$\begin{aligned} I_{\alpha_r ef} &= I_{\alpha_L} - \frac{(P_L - P_{PV})}{(V_\alpha^2 + V_\beta^2)} V_\alpha \\ I_{\beta \mathrm{ref}} &= I_{\beta L} - \frac{(P_L - P_{PV})}{(V_\alpha^2 + V_\beta^2)} . V_\beta \end{aligned} \tag{4.8}$$

It is important to take into account that the replacement $P_L = V_\alpha I_{L\alpha} + V_\beta I_{L\beta}$ was made, where P_L is the load power and P_{PV} is the photovoltaic system nominal power.

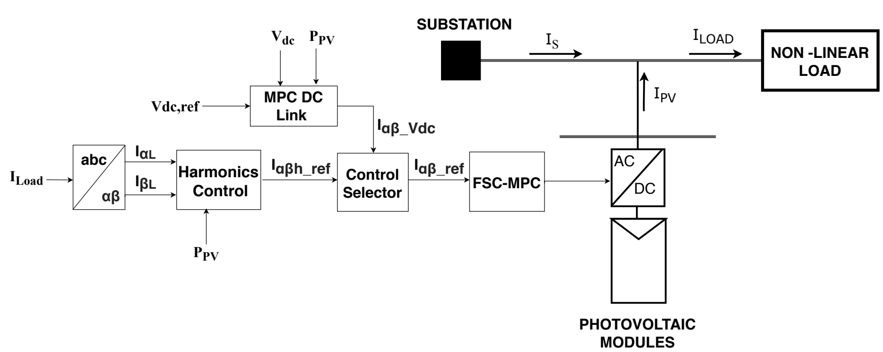

Figure 4.6: Control system for harmonics compensation

Figure 4.6 shows the complete strategy proposed for including harmonics compensation in photovoltaic systems. The strategy consists in the control of the voltage of the dc-link using the MPC proposed in Section 4.2.2, and the control for harmonic compensation applying FCS-MPC. Finally, a control selector has included, wich is responsible for guarantee the compensations of harmonics without neglected the control of the voltage of the dc-link.

4.4 Results of the control for harmonics compensation

The proposed control was simulated in Matlab/Simulink over the tested power electric system show in Figure 4.6, which is based on Colombian voltage levels and includes a non-linear load that injects the harmonics to the grid which we want to reduce. The parameters of the tested electric system and the photovoltaic system are presented in Table 4.2.

PV system power	***Non-linear load power***	V_{dc}	V_{ac}
20kVA	20KVA	2000V	400V

Table 4.2: Parameters of the tested system

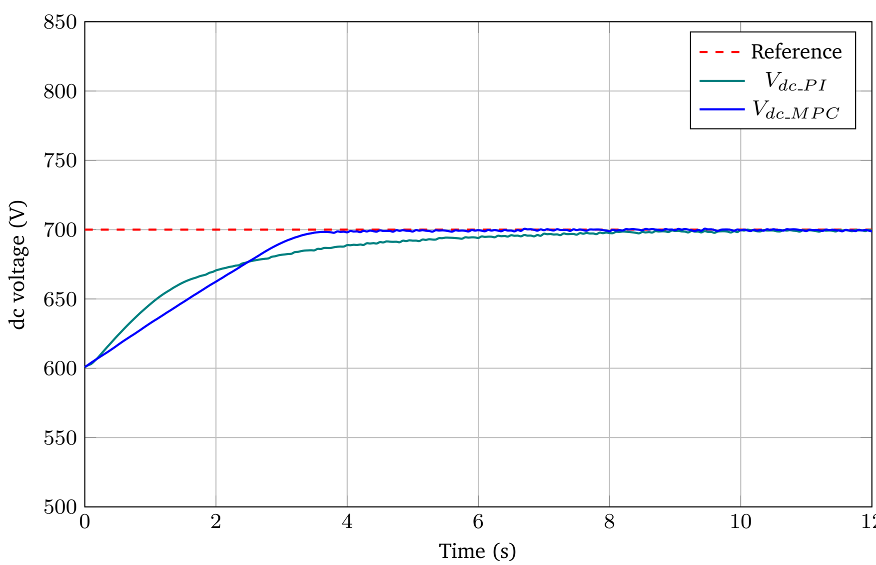

Figure 4.7: Voltage control results of the dc-link

	Settling time
PI controller	8 *ms*
MPC controller	3.5 *ms*

Table 4.3: Results of the dc voltage control

Figure 4.7 shows the results of the voltage control of the dc-link, showing that the PI controller has a settling time of 8 ms while the FCS of the dc-link has a settling time of 3.5 seconds and not has overshoot, demonstrating that

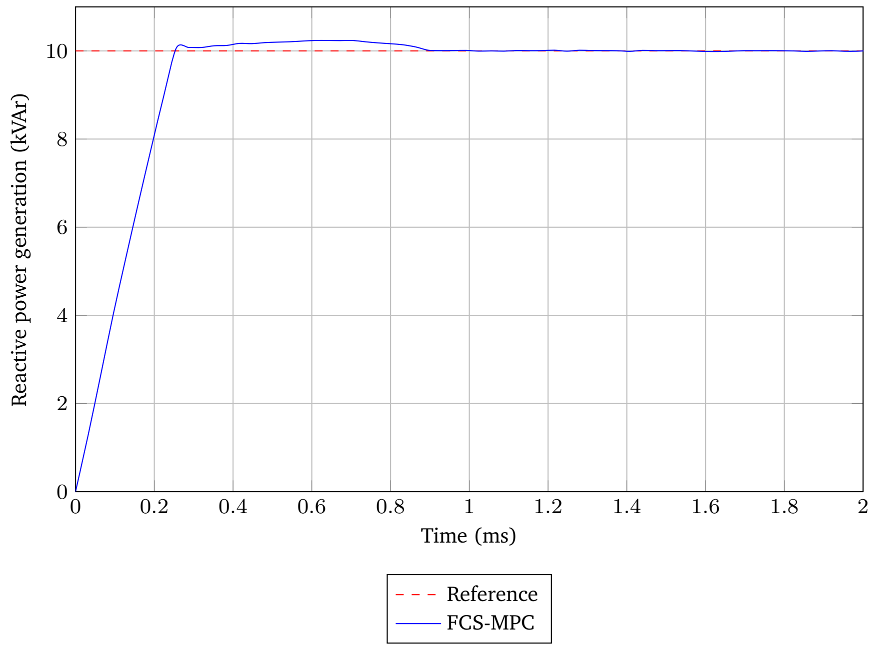

Figure 4.8: Reactive control results

	Overshoot	*Settling time*
FCS-MPC	2.45%	0.93 *ms*

Table 4.4: Results of the reactive control

the proposed control is faster and has a better performance than the PI controller(see Table 4.3).

In addition, Figure 4.8 shows that the control of the reactive power has a settling time of 0.93 ms seconds and a overshoot of 2.45%, showing a fast response and a minimum overshoot(see Table 4.4). It demonstrates that the control system proposed improved the performance of the dc-link control with respect to PI controllers.

Additionally, Figure 4.9 shows the control of the currents I_α and I_β, showing that these currents follow almost perfectly the currents references computes by the control system strategy. Finally, Figure 4.10 shows the performance of the application of the control strategy of the photovoltaic systems for harmonics compensations using FCS-MPC and optimization theory, where the first part pf the figure shows the transient of the sytem influenced by the response of the harmonic compensation of the . The results show that the photovoltaic system with the harmonics compensation function proposed, showing that the THD of the source current was reduced from 15.28$\%$ to 3.26$\%$.

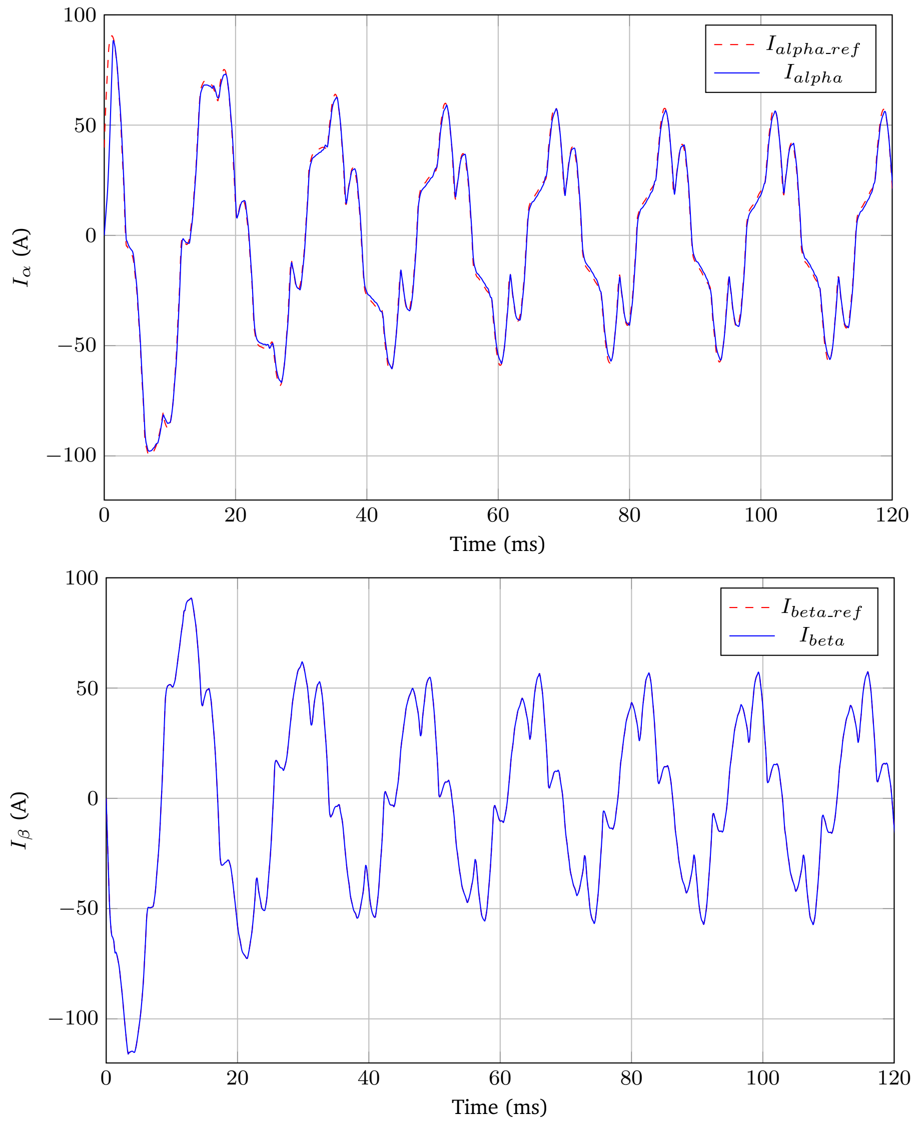

Figure 4.9: Alpha and beta current results

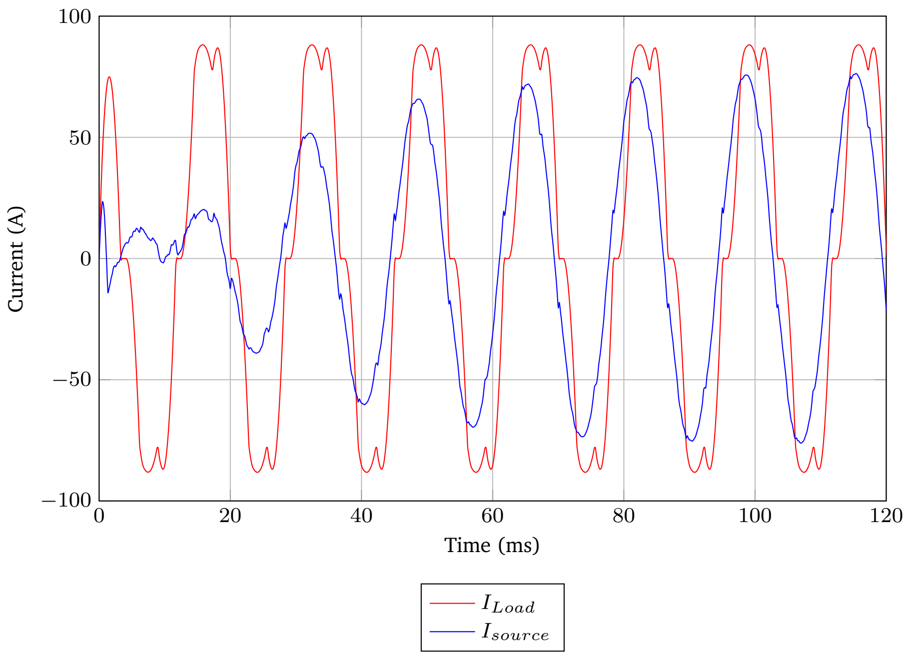

Figure 4.10: Harmonic currents compensation

Chapter 5

Virtual synchronous machine

5.1 The role of synchronous machines in conventional power electric systems

Historically, electrical power systems have been strongly related to the synchronous generator, which is the electric machine that coupled to a turbine has been responsible for making the conversation from mechanical energy to electrical energy in power generation systems. The most popular systems for generation of electric energy are hydroelectric plants and thermal power stations, which represent 63% and 30% of the Colombian electric power generation respectively.

Hydroelectric power plants have as principle the accumulation of potential energy from large bodies of water in a dam and the capture of the energy of the falling water to generate electricity, through a turbine that converts the kinetic energy of falling water into mechanical energy, and finally converts the mechanical energy from the turbine into electrical energy using the synchronous generator.

On the other hand, the thermal power stations generate electrical energy from the heat produced by the combustion of fossil materials such as coal, oil or gas, generating a thermodynamic cycle which uses energy in the form of heat to move the turbines coupled to the synchronous machine and generate electrical energy.

The conventional generation systems, which are dominated by synchronous machines, are connected to the power electric systems through transmission lines composing an interconnecting system working in synchronism as shown in Figure 5.4, and that means that all generators connected to the system work at the synchronous speed that defines the frequency of the electric power system. This interconnection allows to have a better response under disturbance (such as faults, load changes and loss of generators) because of the inertia of the synchronous generators that response instantaneously through the rotating mass, which acts to overcome the imbalance of supply and demand by changing the rotational speed (and the electrical frequency as well), thus the kinetic energy of the unit.

The ability of an electrical power system to remain in a state of equilibrium operation under normal operating conditions and to regain another state of equilibrium after being subjected to a disturbance is known as stability, and it depends on the capacity to maintain a restored equilibrium between electromagnetic and mechanical torques acting on the rotor of each synchronous machine in the interconnected system. Power system stability involves the study of the dynamics of the power system under disturbances. On the other hand, system instability can be seen as loss of synchronism when the system is subjected to a disturbance.

However, in the context of new technologies, renewable energies, and microgrids, the capacity of electric power generation is displacing conventional power generation systems. Unlike conventional systems, which usually use synchronous machines, renewable energy systems have either very small or no rotating mass and damping property, that means a reduction of the total inertia of the systems and affect the stability of the electrical power system.

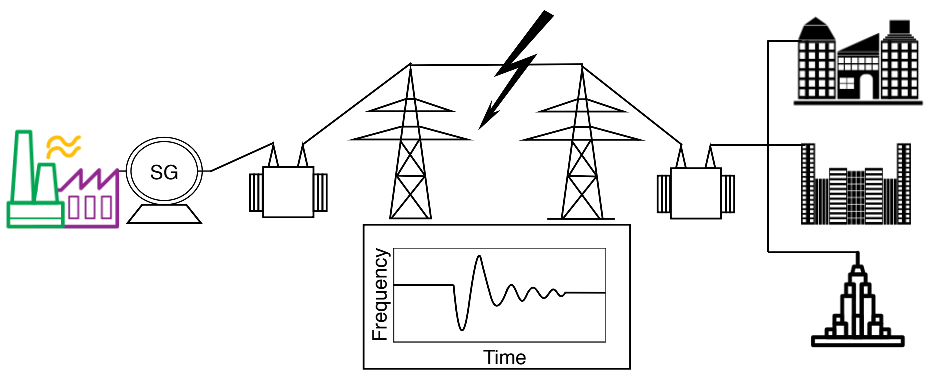

Figure 5.1: The synchronous generator and the frequency response in power electric systems

5.2 Virtual synchronous machine in the context of microgrids

Due to the rapid growth of renewable and distributed energy resources (DER), their impact on the legacy ac grid is becoming an important topic. Usually, they are connected to the ac grid using a dc/ac converter as the interface. However, there are still many major challenges to integrate them into the legacy power (Chen et al., 2017).

1. dc/ac converters using traditional power electronics control strategy have fast dynamics. However, the key equipment in power system: the synchronous machine, has slow dynamics with large inertia. The equivalent rotational inertia of the grid will significantly decrease at high distributed energy resources penetration. This will cause degradation in frequency stability.

2. The power generated by distributed energy resources is intermittent, and will be instantly presented to the grid through fast responding dc/ac converters. These interactions will lead to frequency, angle, and voltage instability. The investigation is also hard for large-scale dc microgrids and dc/ac converters in parallel, especially when the DERs have similar dynamics with the dc/ac converters. Meanwhile, DERs usually work under the maximum power point tracking (MPPT) control and thus are non-dispatchable. So these dc/ac converters cannot provide up-reserve to support the grid frequency.

3. Under all grid conditions, the ac frequencies, voltages of ac grids, and the dc voltages of dc microgrids should be controlled within a safe operation range. Autonomous controls are necessary for the dispatchable units, such as the energy storages in the dc microgrid and the dc/ac converters, to achieve power balancing and sharing.

Compared to the conventional bulk power plants, in which the synchronous machines dominate, the distributed generator (DG) units have either very small or no rotating mass and damping property. With growing the penetration level of DGs, the impact of low inertia and damping effect on the grid stability and dynamic performance increases. A solution towards stability improvement of such a grid is to provide virtual inertia by virtual synchronous generators (VSGs) that can be established by using short term energy storage together with a power inverter and a proper control mechanism. A VSG-based frequency control scheme is addressed, and the paper is focused on the poetical role of VSGs in the grid frequency regulation task.

The capacity of installed inverter-based distributed generators (DGs) in power system is growing rapidly; and a high penetration level is targeted for the next two decades. European countries, USA, China, and India significant targets are also considered for using the DGs and renewable energy sources (RESs) in their power systems up to next two decades. Compared to the conventional bulk power plants, in which the synchronous machine dominate, the DG/RES units have either very small or no rotating mass (which is the main source of inertia) and damping property. The intrinsic kinetic energy (rotor inertia) and damping property (due to mechanical friction and electrical losses in stator, field and damper windings) of the bulk synchronous generators play a significant role in the grid stability. With growing the penetration level of DGs/RESs, the impact of low inertia and damping effect on the grid dynamic performance and stability increases. Voltage rise, because of reverse power from PV generations, excessive supply of electricity in the grid due to full generation by the DGs/RESs, power fluctuations caused by variable nature of RESs, and degradation of frequency regulation (especially in the islanded microgrids) can be considered as some negative results of mentioned issue. A solution towards stabilizing such a grid is to provide additional inertia, virtually. A virtual inertia can be established for

DGs/RESs by using short term energy storage together with a power electronics inverter/converter and a proper control mechanism. This concept is known as virtual synchronous generator. The units will then operate like a synchronous generator, exhibiting amount of inertia and damping properties of conventional synchronous machines for short time intervals (in this work, the notation of VSG is used for the mentioned concept). As a result, the virtual inertia concept may provide a basis for maintaining a large share of DGs/RESs in future grids without compromising system stability (Bevrani et al., 2013).

5.3 Concept of the virtual synchronous machine

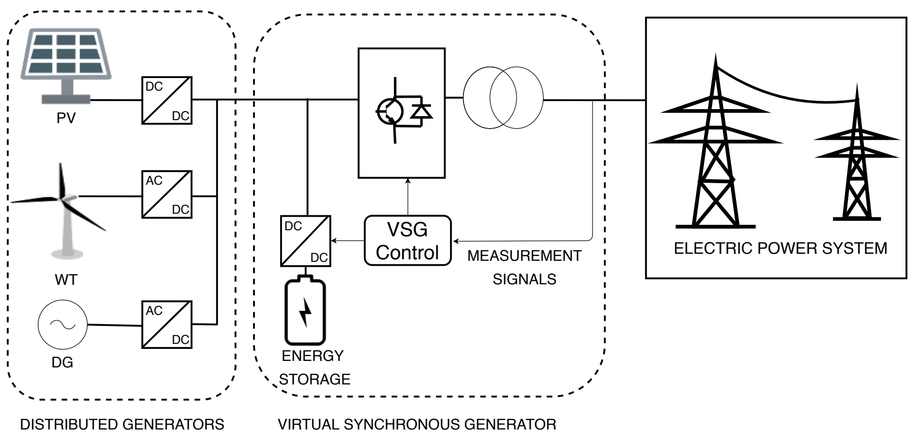

Figure 5.2: General structure of the VSG

The idea of the VSG is initially based on reproducing the dynamic properties of a real synchronous generator (SG) for the power electronics-based DG/RES units, in order to inherit the advantages of a SG in stability enhancement. The principle of the VSG can be applied either to a single DG, or to a group of DGs. The first application may be more appropriate to individual owners of DGs, whereas the second application is more economical and easier to control from the network operator point of view. The dynamic properties of a SG provides the possibility of adjusting the power, dependency of the grid frequency on the rotor speed, and highlighting the rotating mass and damping windings effect as well as stable operation with a high parallelism level. The VSG consists of energy storage, inverter, and a control mechanism as shown in Fig. 5.3 The VSG is usually located between a dc bus/source/DG and the grid. The VSG shows the dc source to the grid as a SG in view point of inertia and damping property.

Actually, the virtual inertia is emulated in the system by controlling the active power through the inverter in inverse proportion of the rotor speed. Aside from higher frequency noise due to switching of inverter's power transistors, there is no difference between the electrical appearance of an electromechanical SG and electrical VSG, from the grid point of view.

The output power of a VSG unit can be simply described as follows:

$$P_{VSG} = P_0 + k_I.\frac{d\Delta\omega}{dt} + k_P.\Delta\omega \tag{5.1}$$

Here $\Delta\omega = \omega - \omega_0$ and ω_0 is the nominal frequency of the grid. The first term of equation (P_0) denotes the primary power that should be transferred to the inverter, the Second term indicates the primary power that should be generated or absorbed by the VSG according to the positive or the negative initial rate of frequency change, where K_I represents the inertia characteristic, and the last term represents the linear damping, where K_P emulates the damper windings.

Since, actually the initial rate of frequency change just provide an error signal (with equilibrium of zero), power will be exchanged only during the transient state without necessarily returning back the frequency of the grid to the nominal value. In order to cover this issue, a frequency droop part should be added as shown in the third term of equation 5.3. The K_p emulates the damper windings effect in a SG, and represents the linear damping.

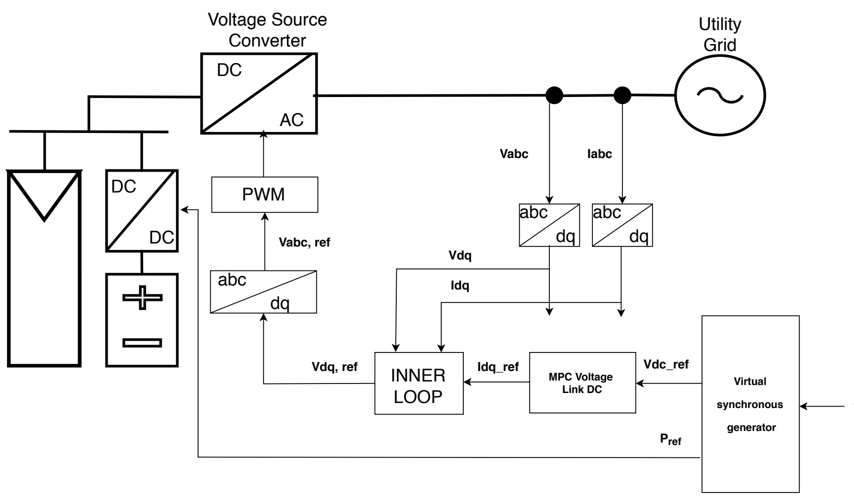

Figure 5.3: Control Including the Concept of VSG

5.4 The structure of the synchronous machine proposed

The power balance in the VSC is similar to synchronous generator, which can be explained through Figure 5.4.

The imbalance power of ac grid will lead to frequency deviation, which could be explained by swing equation 5.2:

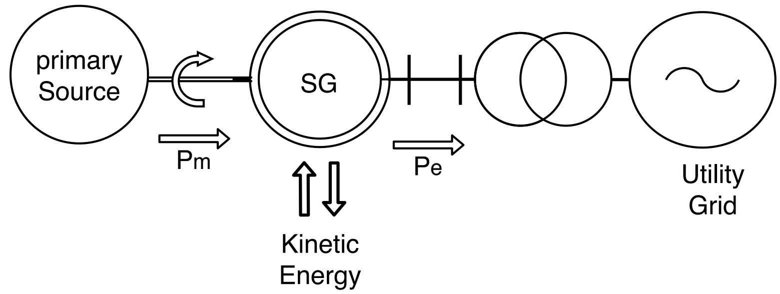

Figure 5.4: Concept of Synchronous Generator

$$2H\frac{d\omega_0}{dt} = P_m^* - P_e^* - D(\omega_0 - \omega) \tag{5.2}$$

where P_m^* and P_e are the prime mover power and the electromagnetic power in per unit values, respectively, H is the inertia constant and D represents the damping factor.

The mismatch between P_m and P_e which is caused by the change of load demand or the disturbance on the prime mover will change the rotor speed. The kinetic energy stored in the rotor could compensate partial of the imbalance power.

With the deceleration (or acceleration) of the rotor speed, the governor of the generator will take a sequence of actions to adjust the position of valve of steam turbine. Thus the power output of prime mover will be adjusted until the system reaches a new equilibrium point.

There is a similar feature for the VSC as shown in Figure 5.5. The power injected by the dc grid can be thought as the prime mover power and the power output of the VSC can be considered as the electromagnetic power. In consideration of the fluctuation of the primary energy (wind, solar, etc.), the dc voltage will change instantly as long as the VSC did not timely adjust its reference power.

The energy stored in the dc capacitors will compensate partial of the imbalance power (Weiyu et al., 2017), which could be explain by the following equation 5.3, where the S_{VSC} is the rated power capability of VSC-station; P_{rec} represents the rectifier power input to VSC system; P_{inv} is the VSC power output to ac grid; C represents the capacitance of dc capacitors; V_{dc} is the dc voltage of the dc-link.

$$\frac{CV_{dc}}{S_{VSC}}\frac{dV_{dc}}{dt} = P_{rec} - P_{inv} \tag{5.3}$$

According to equation 5.3, the $V^2 - P$ control method can be derived as follows:

$$\Delta P = K_{\text{droop}}\Delta V_{dc}^2 \tag{5.4}$$

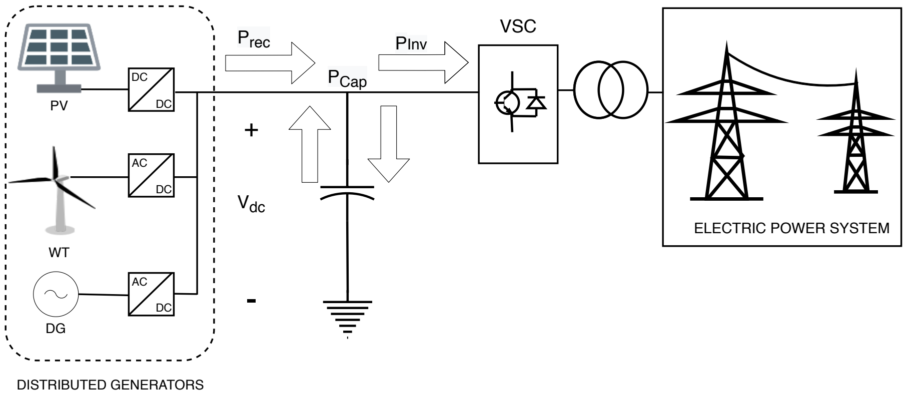

Figure 5.5: Control including the concept of VSG

Where K_{droop} is the droop coefficient; ΔV_{dc}^2 is the dc voltage deviation and the ΔP is the additional power signal for VSC. The K_{droop} determines the power allocation ratio of the VSC system. However, K_{droop} will keep constant in a relatively short period until the transmission system operator (TSO) change it. Thus, traditional $V^2 - P$ control method is unable to provide oscillation damping or fast frequency support. Equation 5.4 indicates that VSC will get more power by the adjustment of the dc reference voltage. With this characteristic, the dc reference voltage would change with the frequency deviation in order to provide frequency support, which is just like the adjustment of prime mover's valve.

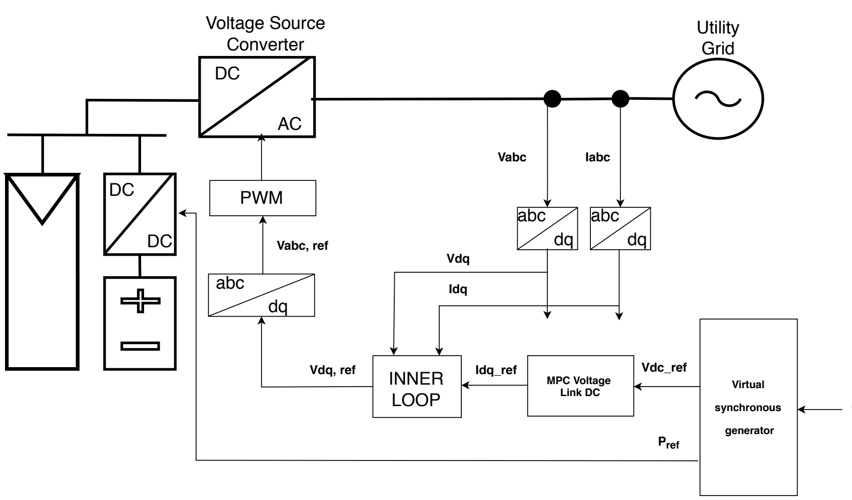

Figure 5.6: General structure of the VSG

5.5 Results of the application of the concept of the synchronous virtual machine

From the results shows in Fig. 5.8 we can conclude that the effect of the concept of the virtual Synchronous Machine improve the response of frequency of the distribution system tested. Specifically, the application of the concept of the virtual synchronous machine proposed reduce the settling time after the connection of the big load from 60 ms to 20 ms, which means a reduction of 67% of the settling time.

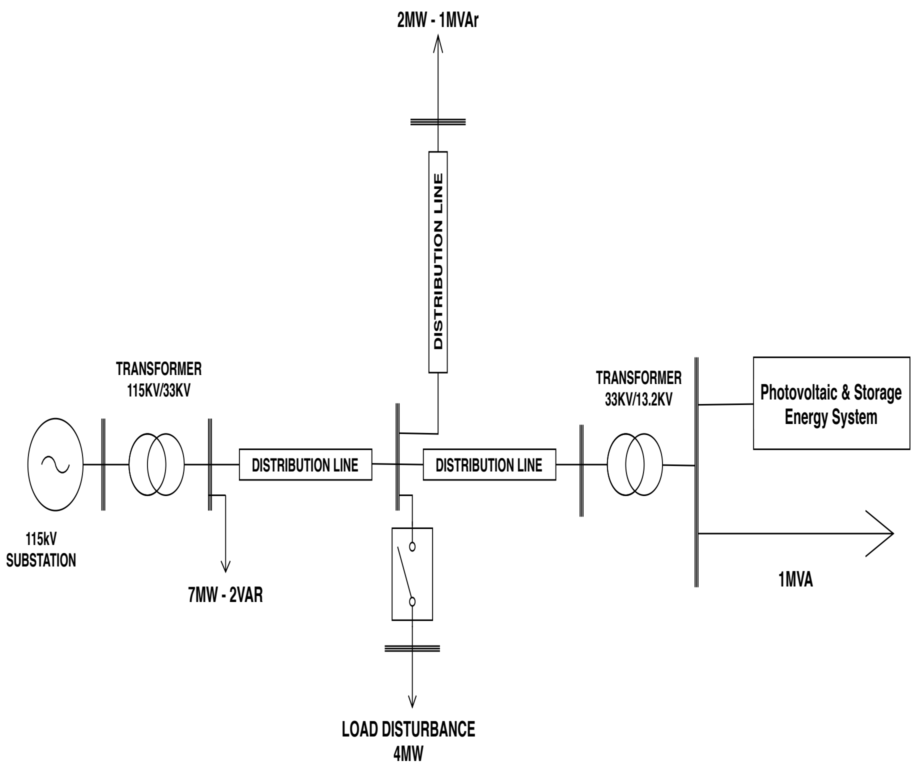

Figure 5.7: Distribution tested for the concept VSG

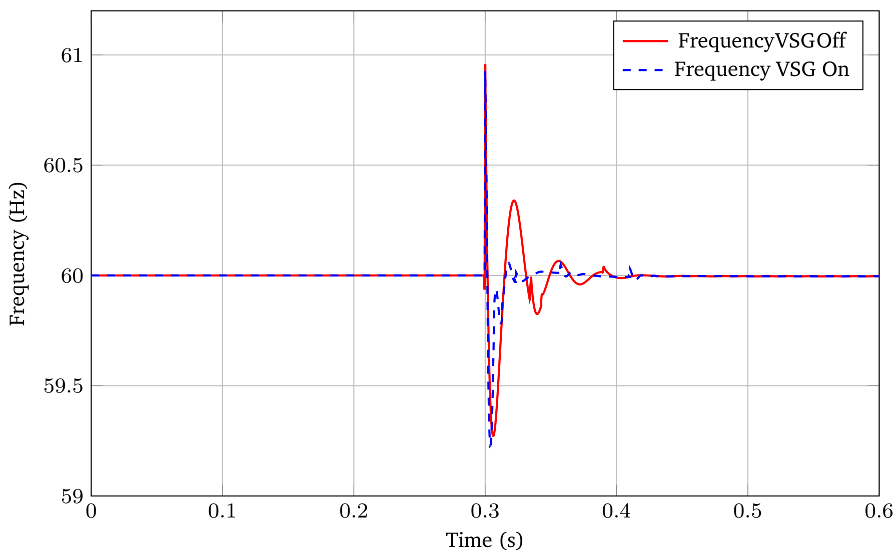

Figure 5.8: Frequency control results of VSG application

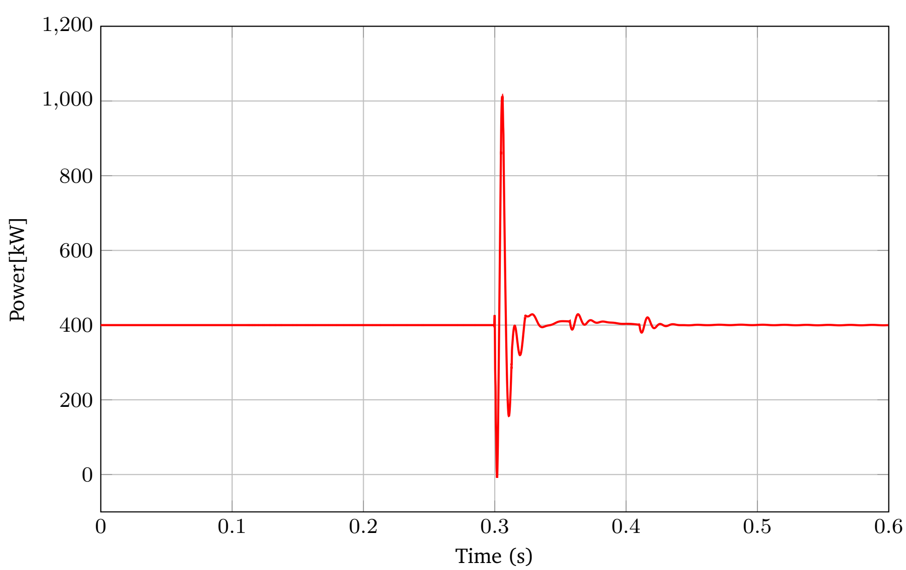

Figure 5.9: Power injected to the grid

Chapter 6

Conclusions

- A deep review of control strategies of converters for batteries energy storage and photovoltaic systems were presented in this thesis. From the simulation results shows in Chapter 3, it is concluded that the dc voltage controller using model predictive control has a faster and better performance than the PI controller. Moreover, the control system proposed for the reactive power of the VSC was satisfactory, showing a more clean signal and a shorter time in the settling than the PI control strategy. In addition,the implementation over a weak distribution network demonstrated that the voltage profile could be improving with a fast response time through the control of the reactive power of storage energy and photovoltaic generation systems.

- The theory of classic control strategies, optimal control techniques, model predictive control and finite control set control and their applications on power electric converters were reviewed in Chapter 4, and the conventional control of photovoltaic systems was modified in order to apply model predictive control and finite control set in order to include the function of harmonics compensation. From the simulation results, it is concluded that the dc Voltage controller using the model predictive control proposed has a faster and better performance than the PI Controllers. Finally, the control of photovoltaic systems proposed for harmonics compensation demonstrated that the strategy control proposed improved the total harmonics distortion current, reducing the THD of the source current from 15.28% to 3.26%.

- From the results in Chapter 5, we can conclude that the effect of the concept of the virtual synchronous machine improve the response of frequency of the distribution system tested. Specifically, the application of the concept of the virtual synchronous machine proposed reduce the settling time after the connection of the big load from 60 ms to 20 ms, which means a reduction of 67% of the settling time.

Appendix A

Synchronous reference frame

The control vector uses in photovoltaic systems consists of transforming the three-phase current and voltage system into a reference frame that rotates synchronously with the grid voltage that rotates synchronously and it is equivalent of a dc system as shown in Fig. A.1, allowing to simplify the control of the photovoltaic system. The transformation of the three phase abc system into the dq reference system is done in the following way: The three phase components $x_a(t)$, $x_b(t)$ and $x_c(t)$ are first described as two vectors in the $\alpha\beta$ reference frame by means of Clark's transformation and then the vectors x_α and x_β are transformed to the synchronous $dq-$reference frame by means of the Park transformation.

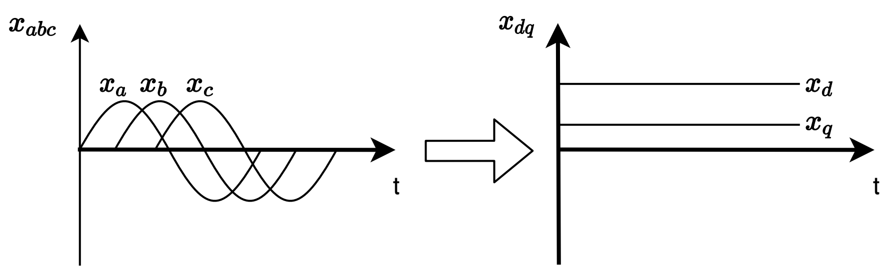

Figure A.1: Synchronous reference frame

Clark transformation

The Clark transformation, also known as $\alpha\beta-$transformation, is used to transform parameters from a three phase system to a system of a two dimensional stationary reference frame, as seen in Figure A.2.

In three-phase systems, the quantities are translated into their two-dimensional orthogonal reference space vectors, together with an ”angle” $\Theta(t)$ with respect

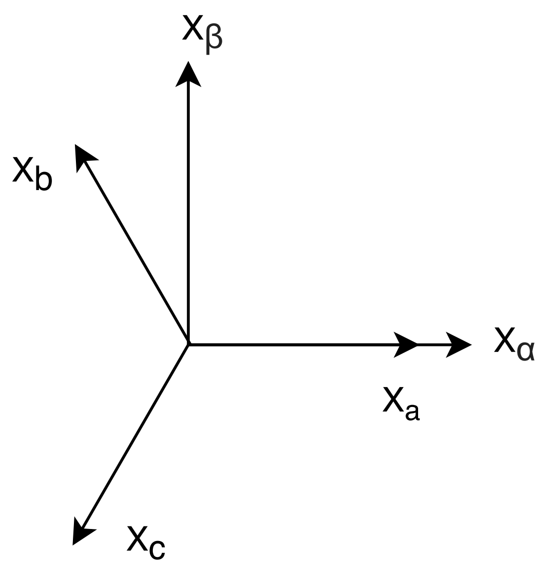

Figure A.2: Conversion of the stationary reference frame abc to $\alpha\beta$

to their reference vectors. Therefore, the number of stationary variables is reduced from the three individual components to two stationary frame components, which allows simpler design and congruence criteria. The vectors $X_\alpha(t)$ and $X_\beta(t)$ rotate with the angular frequency $\omega(t)$, which is the angular frequency of the voltage network in rads.

The Clark transformation can be made in two different ways, power invariant transformation and amplitude invariant transformation. However, this work uses the amplitude invariant Clark Transformation.

The Clark transformation of the system is done by using the following transformation:

$$\begin{pmatrix} X_\alpha(t) \\ X_\beta(t) \end{pmatrix} = \frac{2}{3} \begin{pmatrix} 1 & -\frac{1}{2} & -\frac{1}{2} \\ 0 & \frac{\sqrt{3}}{2} & -\frac{\sqrt{3}}{2} \end{pmatrix} \begin{pmatrix} X_a \\ X_b \\ X_c \end{pmatrix} \tag{A.1}$$

Park transformation

The most common mathematical representation of voltage source converters involves the Park transformation in order to eliminate the time-variant dependence of the dynamical system when it is modeled using abc reference frame. In this structure, Park transformation is used to transform an $\alpha\beta$-reference to dq-reference by means of the matrix equation A.2:

$$\begin{bmatrix} X_d(t) \\ X_q(t) \end{bmatrix} = \begin{bmatrix} \cos(\theta(t)) & \sin(\theta(t)) \\ -\sin(\theta(t)) & \cos(\theta(t)) \end{bmatrix} \begin{bmatrix} X_\alpha(t) \\ X_\beta(t) \end{bmatrix} \tag{A.2}$$

The vectors $X_d(t)$ and $X_q(t)$ represent currents, where $X_d(t)$ is the current that provides the required power to the dc bus and $X_q(t)$ is the current that defines the reactive power condition. This transformation gives excellent control possibilities. A correct transformation requires an exact value of the angle $\theta(t)$ to uncouple the components for an independent power control.

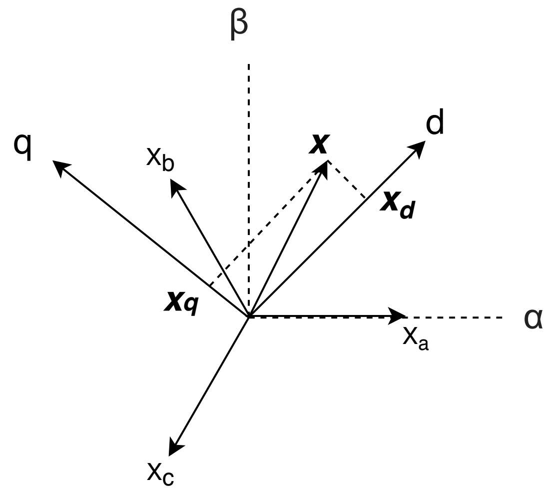

Figure A.3: Conversion of the stationary reference frame $\alpha\beta$ to the dq synchronous Reference frame

The value of the angle ($\theta(t)$) is calculated by a synchronization technique, specifically the phase-locked loop (PLL) is used. In addition, the phase lock loop is used to synchronize switching power devices, calculate and control the active/reactive power flow by transforming the feedback variables into a suitable reference frame for control purposes.

Appendix B

Codes and examples of model predictive control

This example shows the SISO model of the dc-link of the voltage source converter simulated in a space state model. The model has the component of the current I_d as the input and the voltage of the dc-link V_{dc} as the output, and the matrices A , B and C are calculated with the parameters of the system. The model is simulated in SIMULINK/MATLAB, however, the parameters of the system are computed in the editor of matlab.

Code of the parameters calculations of the the dc-link SISO Model

```
Ts=10/60;
C=1;
Vdc=1;
Id=0.88;
Vd=1;
P0=1;
Vd=1;
A=(1/(C*Vdc)^2)*(P0-(3*Vd*Id)/2);
B=3*Vd/(2*C*Vdc);
C=1;
D=0;
plantt=ss(A,B,C,D);
pd=c2d(plantt,Ts);
Ap=pd.A;
Bp=pd.B;
Cp=pd.C;
Dp=pd.D;

Ac=exp(A*Ts)
```

```
Bc=(B/A)*(exp(A*Ts)-1)
n = 1;  % State variables (x)
m = 1;  % Control variable (u)
N = 20; % Horizon window
y_ref = 1*ones(m,1);
u_ref=inv(Cp*inv((eye(n) - Ap))*Bp)*y_ref;
W=kron(ones(N,1),u_ref);

% MPC Parameters
Q=0.02*eye(N*m);
R = kron(ones(N,1),y_ref);

h=zeros(m*N,n+m);
Fb(1:m,:)=Cp*Ap;

for kk=m+1:m:m*N
Fb(kk:kk+m-1,:)= Fb(kk-m:kk-1,:)*Ap;
end

Gb = [Bp];

for k = 1:(N-1)
    Gb = [Gb,zeros(k*n,m);Ap*Gb(k*n-n+1:end,:),Bp];
end
Gb = kron(Cp,eye(N))*Gb;
```

The simulation is run in SIMULINK/MATLAB through the next block diagram show in Figure B.1:

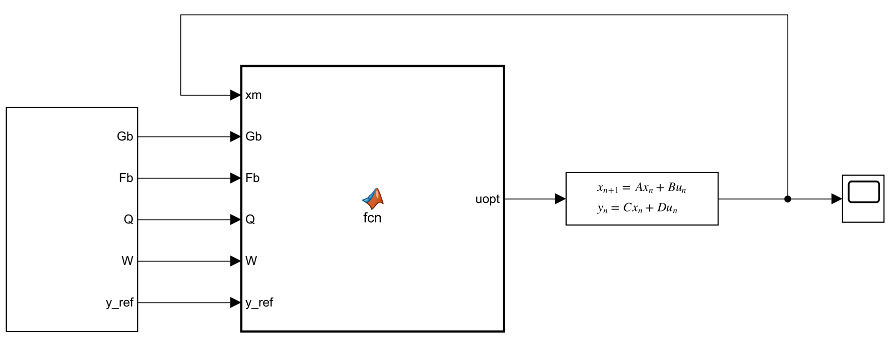

Figure B.1: Simulink Simulation

The Matlab function (fcn) that compute the optimal output in each iteration using Equation 3.7 of the concept of model predictive control shows in this appendix.

Code of the Matlab funtion

```
function uopt = fcn(xm,Gb,Fb,Q,W,y_ref)
N=20;
R = kron(ones(N,1),y_ref);
U=inv(Gb'*Gb+Q)*(Q*W+Gb'*R-Gb'*Fb*xm);
uopt=U(1,:);
```

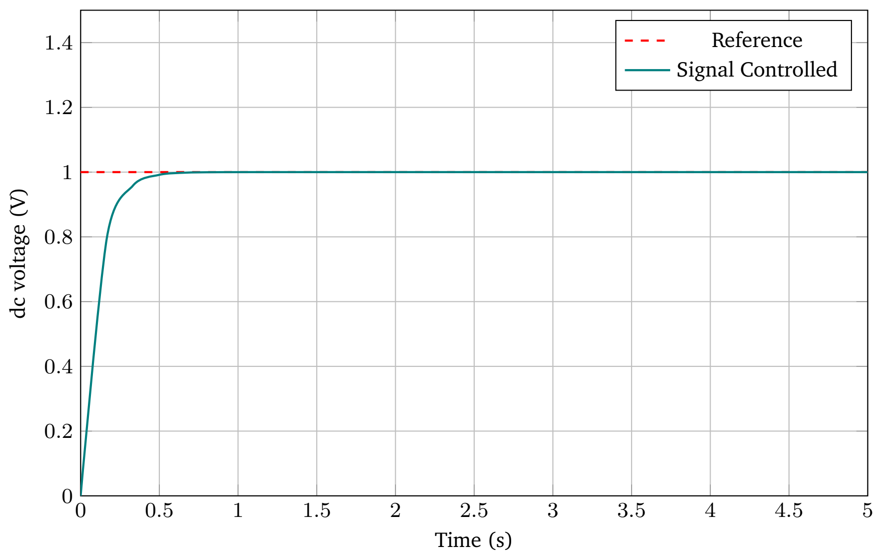

Figure B.2: SISO example

Example: Control of a MIMO model

This example shows the performance of model predictive control apply in an hypothetical MIMO space state system of 3 inputs and 3 outputs with a horizon window of 10 steps.

```
%% MIMO system
n = 3;  % State variables (x)
m = 3;  % Control variables (u)
N = 10; % Horizon window
Ap = [-0.1357     0.3715     0.4748
       0.0323    -0.1713    -0.4240
```

```
      0.2117        0.1501       0.0870];
Bp = [-0.0861      0.2588      0.2811
      -0.1909      0.4952     -0.3042
      -0.2362     -0.3134      0.4924  ];
Cp = eye(m,n);
Dp=zeros(3);

% references
y_ref = 10*ones(m,1);
u_ref=inv(Cp*inv((eye(n) - Ap))*Bp)*y_ref;
W=kron(ones(N,1),u_ref);
%% MPC Parameters
Q=1000*eye(N*m);
R = kron(ones(N,1),y_ref);

Fb = [];
for k = 1:N
    Fb = [Fb;Cp*(Ap^k)];
end
Gb = [Bp];

for k = 1:(N-1)
    Gb = [Gb,zeros(k*n,m);Ap*Gb(k*n-n+1:end,:),Bp];
end
Gb = kron(Cp,eye(N))*Gb;
```

Matlab function

```
function uopt = fcn(xm,Gb,Fb,Q,W,y_ref)
N=10;
R = kron(ones(N,1),y_ref);
U=inv(Gb'*Gb+Q)*(Q*W+Gb'*R-Gb'*Fb*xm);
uopt=U(1:3,:);
```

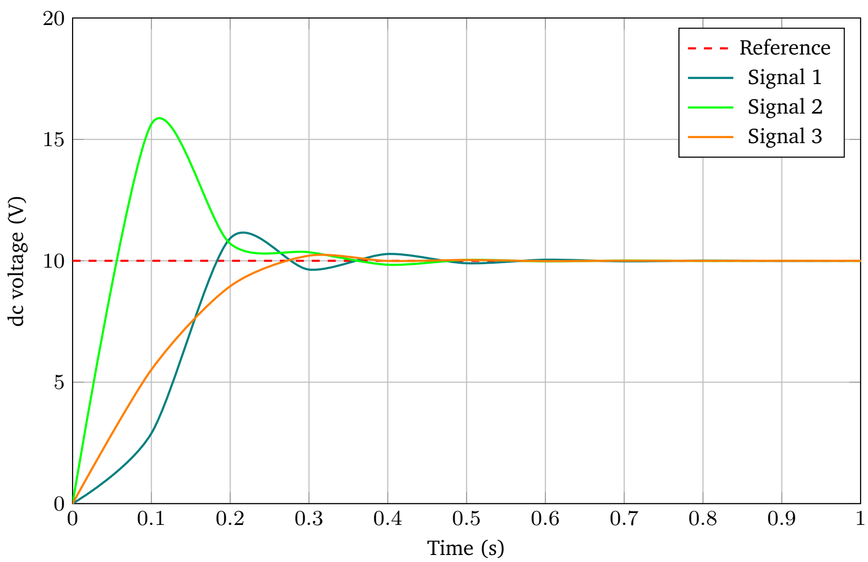

Figure B.3: MIMO example

Appendix C

Standard and national regulation about power quality

Two power quality issues are important for the integration of photovoltaic systems, namely, voltage events and harmonic distortion. Each of these problems are briefly presented below in relation to the standard IEEE 519 (IEEE, 2014).

C.1 Voltage events

Voltage events are divided into short and long duration events. In Colombia, the steady state voltages at 60 Hz may not be less than 90% of the nominal voltage nor exceed 110% of this for a period of more than one minute. In the case of systems with a nominal voltage equal to or greater than 500 kV, they may not exceed 105%, for a period of more than one minute. Long-term events are classified as follows:

- **Long-term interruptions (Sustained interruptions):** These are voltage drops or voltage cancellations of the electrical network, which occur when the voltages are less than 0.1 p.u and last longer than one minute.
- **Long-term voltage drop (Under voltage):** These are long-term voltage events lasting longer than 1 min and a voltage level between 10% and 90% of the system nominal voltage.
- **Under voltage:** Long-term voltage events greater than 1 min and a voltage level 10% above the nominal system voltage.

On the other hand, voltage fluctuations are phenomena that cause the transient distortion of the voltage waveform, with respect to its standard form. A discontinuity of service is said to exist when the voltage does not follow the standard waveform. The voltage fluctuations are summarized in Table C.1 and are classified into the following types:

- **Sag:** Voltage fluctuation characterized by producing a transient voltage depression with respect to the standard wave.
- **Swell:** Voltage fluctuation characterized by producing a transient increase in voltage with respect to the standard wave.
- **Flicker:** Impression of instability of visual sensation caused by a light stimulus, whose luminosity or spectral distribution fluctuates over time. The indicator of the perceptibility of an equipment or system (PST), allows evaluating voltage fluctuations over a short period of time (10 minutes), obtained statistically from the treatment of the voltage signal. The way to calculate it is defined in the Standard IEC-61000-4-15 (2003-02).

Table C.1: Classification of short-term events

Categories	***Duration***	***Magnitude(p.u.)***
Instantaneous		
Instantaneous Sags	0.5 - 30 cycles	0.1 - 0.9
Instantaneous Swells	0.5 - 30 cycles	1.1 - 1.8
Momentary		
Momentary Interruptions	0.5 cycles - 3 s	< 0.1
Momentary Sags	0.5 cycles - 3 s	0.1 - 0.9
Momentary Swells	0.5 cycles - 3 s	0.1 - 1.4
Temporary		
Temporary Interruptions	3s - 1min	< 0.1
Temporary Sags	3s - 1min	0.1 - 0.9
Temporary Swells	3s - 1min	

C.2 Total harmonic voltage distortion(THDV)

Harmonics are sinusoidal voltages or currents having frequencies that are whole multiples of the frequency at which the supply system is designed to operate, which corresponds to 60 Hz in Colombia. The main sources of harmonics are no linear loads such as power electronic converters, Low power consumption lamps, current regulators, electrical arc-furnaces, among others. Harmonics affect mainly capacitors, transformers, and motors, causing additional losses, overheating, and overloading.

The total harmonic distortion of voltage index allows to measure the deformation of the voltage wave with respect to the standard wave, expressed as a percentage. The way to calculate it is defined in IEEE Standard 519.

In accordance with number 6.2.1.2 of appendix 1 of resolution 024-2005 (CREG-024-2005, 2005) of Comisión de regulación de energía y gas de Colombia (CREG), Colombian utilities must comply with the requirements established in Table C.2 of said number, which is based on The maximum limits for total voltage distortion of IEEE standard 519-1992.

Table C.2: THDV limits in Colombia

Voltage system	***THDV limit***
1kV$<$ Voltage $<$ 57.5kV	5%
57.5kV$\leq$ Voltage $<$ 220kV	2.5%
Voltage $\geq$ 220kV	1.5%

C.3 Power factor and reactive power managment

The main effect of reactive power flow in electric power systems are the losses because of the Joule effect and voltage regulation problems. In general terms, reactive power are related with voltage stability: decreasing reactive power causes voltage to fall while increasing it causes voltage to rise.

In accordance with resolution 108-1997 of CREG, the inductive power factor of the installations must be equal to or greater than point ninety (0.90). The utilities will require those facilities whose inductive power factor violates this limit, to install appropriate equipment to control and measure reactive energy (CREG-108-1997, 1997). In addition, the capacitive power factor was limited through the resolution 015-2018 of CREG, and according to this resolution, the cost of reactive energy transportation will be made based on the following expression (CREG-015-2018, 2018):

$$CTER_{u,n,h,m,j} = ER_{u,h,m,j} * M * D_{n,h,m}$$

Where:

- $CTER_{u,n,h,m,j}$: Cost of transporting reactive energy in excess of the limit assigned to the user of the distribution or transmission system u, in Colombian pesos, of the voltage level n, in hour h of month m, of the system operated by utility j.

- $ER_{u,h,m,j}$: Amount of reactive energy transported in excess of the limit assigned to the user of the distribution or transmission system u, in the hour h of the month m, in the utility system j, in $kVAr$.

- $D_{n,h,m}$: Charge for the use of distribution systems for the transport of reactive energy. It is equal to the charge for use of voltage level n in hour h of month m that a user connected to the system faces, when the transport of reactive energy was registered. The applicable use charge for the payment of the reactive energy transport by the user of the the distribution or transmission system will be equal to the charge for the use of active energy that it faces depending on the system and the voltage level at which the border is connected.

- M: Variable associated with the monthly period in which the transport of reactive energy occurs over the established limit, varying between 1 and 12. When the transport of reactive energy in excess of the limit occurs during any hourly period in ten (10) days or less in the same calendar month, variable M will be equal to 1. When the transport of reactive energy in excess of the limit occurs during any hour period in more than ten (10) days in the same calendar month, variable M it will be equal to 1 during the first 12 months in which this condition occurs and, from the thirteenth month of reactive energy transport with the same condition, this variable will increase monthly by one unit until reaching the value of 12. If the condition disappears for more than six consecutive months, the variable will restart from 1.

The payment of the cost of reactive energy transportation must be made when an utility or an end user is involved in any of the following conditions :

(a) When the inductive reactive energy (kVArh) consumed by an utility is greater than fifty percent (50%) of the active energy (kWh) that is delivered to it in each hourly period at voltage levels 3, 2 or 1. In this In this case, to calculate the excess transport of reactive energy, the hourly reactive energy of the border points of the same system must be added, understanding as the border point the connection points with other systems (utilities) at the same level of tension. The balance will be calculated based on the arithmetic sums, considering the direction of the active and reactive energy flows through said border points. The payment will be distributed among the utilities that transport said reactive energy in proportion to the amount of reactive power transported.

(b) When an end user registers at their commercial border an inductive reactive energy consumption of more than fifty percent (50%) of the active energy (kWh) that is delivered in each hourly period. In the event that the active energy is equal to zero in any period and there is inductive reactive energy transport, the cost of reactive energy transport will be made on all the reactive energy registered in said period.

(c) When the transport of capacitive reactive energy is registered at a commercial border, regardless of the value of active energy, the cost of transporting reactive energy will be charged on all the registered reactive energy.

C.4 Small-scale self-generation and distributed generation capacity limits

The Colombian regulation through the resolution CREG-030-2018 limits the capacity of Small-scale self-generation and distributed generation in order to avoid voltage fluctuations and reverse power flows mentioned previously, among other issues related to the protection and control of distribution systems, CREG set the next limitations:

a) The sum of the installed power of the GD or AGPE that deliver energy to the network must be equal to or less than 15 % of the nominal capacity of the circuit, transformer or substation where the connection point is requested. The nominal capacity of a network is determined by the capacity of the transformer.

b) The amount of energy in one hour that can be delivered by the GD or AGPE that deliver energy to the grid, whose energy production system is different from that of photovoltaic without storage capacity, connected to the same circuit or transformer, must not exceed 50 % of annual average of the hours of minimum daily energy demand registered for the year prior to the request for connection.

c) The amount of energy in one hour that can be delivered by the GD or AGPE that deliver energy to the grid, whose energy production system is composed of photovoltaic without storage capacity, connected to the same circuit or voltage level transformer 1 , must not exceed 50 % of annual average of the hours of minimum daily energy demand registered for the year prior to the request for connection in the time zone between 6 am and 6 pm.

Bibliography

Anderson, P. M. (1995). *Power Systems Control and Stability*. IEEE press.

Bajracharya., C. (2008). Control of vsc-hvdc for wind power. Master's thesis, Norwegian University of Science and Technology.

Barutcu, Cagri, I., Karatepe, Engin, and Boztepe, M. (2020). Impact of harmonic limits on pv penetration levels in unbalanced distribution networks considering load and irradiance uncertainty. *International Journal of Electrical Power & Energy Systems*, 118:105780.

Benadli, R., Khiari, B., and Sellami, A. (2015). Three-phase grid-connected photovoltaic system with maximum power point tracking technique based on voltage-oriented control and using sliding mode controller.

Bevrani, H., Ise, T., and Miura, Y. (2013). Virtual synchronous generators: A survey and new perspectives. 54:244–254.

Chen, D., Xu, Y., and Huang, A. (2017). Integration of dc microgrids as virtual synchronous machines into the ac grid. 64:7455–7466.

Cortes, P., Kazmierkowski, M., Kennel, R., Quevedo, D., and Rodriguez, J. (2008). Predictive control in power electronics and drives. *IEEE Transactions on Industry Applications*, 55:1380 – 1389.

CREG-015-2018 (2018). Metodología para la remuneración de distribución de energía eléctrica. *Comisión de Regulación de Energía y Gas*.

CREG-024-2005 (2005). Normas de calidad de la potencia eléctrica aplicables a los servicios de distribución de energía eléctrica. *Comisión de Regulación de Energía y Gas*.

CREG-030-2018 (2018). Autogeneración a pequeña escala y generación distribuida. *Comisión de Regulación de Energía y Gas*.

CREG-108-1997 (1997). Criterios generales sobre protección de los derechos de los usuarios de los servicios públicos domiciliarios de energía eléctrica y gas combustible por red física, en relación con la facturación, comercialización y demás asuntos relativos a la relación entre la empresa y el usuario, y se dictan otras disposiciones. *Comisión de Regulación de Energía y Gas*.

Delavari, A., Kamwa, I., and Zabihinejad, A. (2016). A comparative study of different multilevel converter topologies for high power photovoltaic applications.

Demirok, E., Casado, P., Frederiksen, K., Sera, D., Rodriguez, P., and Teodorescu, R. (2011). Local reactive power control methods for overvoltage prevention of distributed solar inverters in low-voltage grids. *IEEE Journal of Photovoltaics*, 2:174 – 182.

Desai, E. and Shah, N. (2013). Comparative analysis of multilevel inverter topologies for photovoltaic system.

Dragicevic, T., Alhasheem, M., Lu, M., and Blaabjerg, F. (2017). Improved model predictive control for high voltage quality in microgrid applications. ieee energy conversion congress and exposition (ecce).

Dwi, C., Hariyanto, N., and Ganjavi, R. (2019). Adaptive protection of distribution systems with ders considering consumer and generation profiles.

Ezequiel, C. (2016). *Modelado lineal de Sistemas de Potencia. Aplicación al Análisis de Estabilidad de Pequeña Señal*. PhD thesis, Universidad nacional de la plata.

Farrokhabadi, M., Konig, S., Canizares, C., Bhattacharya, K., and Leibfried, T. (2018). Battery energy storage system models for microgrid stability analysis and dynamic simulation.

Garces, A., Molinas, M., and Rodriguez, P. (2012). A generalized compensation theory for active filters based on mathematical optimization in abc frame. *Electric Power Systems Research*, 90:1 – 10.

Geyer, T. (2011). A comparison of control and modulation schemes for medium-voltage drives: Emerging predictive control concepts versus pwm-based schemes. *IEEE Transactions on Industry Applications*, 47:1380 – 1389.

Holmes, D. G. and Lipo, T. A. (2003). *Pulse Width Modulation For Power Converters: Principles and Practice*. John Wiley and Sons.

IEEE (2014). Ieee recommended practice and requirements for harmonic control in electric power systems. *IEEE Std. 519-2014*, pages i –29.

Kalitjuka, T. (2011). Control of voltage source converters for power system applications. Master's thesis, Norwegian University of Science and Technology.

Koyanagi, K., Y. Hida, Y. I., Yoshimi, K., Yokoyama, R., Inokuchi, M., Mouri, T., and Eguchi., J. (2011). A smart photovoltaic generation system integrated with lithium-ion capacitor storage. *International Universities' Power Engineering Conference*.

Li, B., Wu, H., and Gao, X. (2011). Investigation of protection schemes for high penetration rooftop photovoltaic system.

Moondee, W. and Shah, N. (2019). Study of coordinated reactive power control for distribution grid voltage regulation with photovoltaic systems.

Mulugeta, T. (2012). *Control, Dynamics and Operation of Multi-terminal VSC-HVDC Transmission Systems.* PhD thesis, Norwegian University of Science and Technology.

Panten, N., Hoffmann, N., and Fuchs, F. W. (2015). Finite control set model predictive current control for grid-connected voltage-source converters with lcl filters: A study based on different state feedbacks. *IEEE Transactions on Power Electronics*, 31:5189 – 5200.

Podder, A. K. and Habibullah, M. (2016). Model predictive control of multi functional inverter for grid tied photovoltaic generators. international conference on power systems (icps).

Rodriguez, T., Kazmierkowski, M. P., Espinoza, J. R., Zanchetta, P., Abu-Rub, H., Young, H. A., and Rojas, C. A. (2013). State of the art of finite control set model predictive control in power electronics. *IEEE Trans. Industrial Informatics*, 9:1003–1016.

R.Teodorescu, Liserre, M., and Rodriguez, P. (2011). *Grid Converters for Photovoltaic and Wind Power Systems*. John Wiley and Sons.

Song, R., Zheng, C., Li, R., and Zhou, X. (2005). Vscs based hvdc and its control strategy.

T., S. and S.Mishra (2018). Model predictive based energy efficient control of grid-connected pv systems. international conference on electrical and computer engineering (icece).

Useche, M., Garces, A., and Rivera, M. (2019). Control of energy storage and photovoltaic systems using model predictive control. In *2019 International Conference on Smart Energy Systems and Technologies (SEST)*, pages 1–6.

van Wesenbeeck, M., de Haan, S., Varela, P., and Visscher., K. (2009). Grid tied converter with virtual kinetic storage. *IEEE Bucharest PowerTech*.

Vargas, J. M. (2007). Control predictivo multivariable: evolución histórica y conceptos.

Wang, P. (2008). *Model Predective Control System Design and implementation using MATLAB*. Springer.

Weiyu, W., Fang, L., Yi, T., Jinhua, H., Shengwei, T., Yong, L., and Yijia, C. (2017). Virtual synchronous generator strategy for vsc-mtdc and the probabilistic small signal stability analysis. 50-1:5424–5429.

Zhang, H., Zhou, H., Reng, J., Liu, W., Ruan, S., and Gao, Y. (2009). Three-phase grid-connected photovoltaic system with svpwm current controller.